

COSMIC HISTORIES OF STARS, GAS, HEAVY ELEMENTS, AND DUST IN GALAXIES

Yichuan C. Pei, S. Michael Fall, and Michael G. Hauser

Space Telescope Science Institute, 3700 San Martin Drive, Baltimore, Maryland 21218

Received 1998 November 5; accepted 1999 April 21

ABSTRACT

We investigate a set of coupled equations that relates the stellar, gaseous, chemical, and radiation contents of the universe averaged over the whole population of galaxies. Using as input the available data from quasar absorption-line surveys, optical imaging and redshift surveys, and the *COBE* DIRBE and FIRAS extragalactic infrared background measurements, we obtain solutions for the cosmic histories of stars, interstellar gas, heavy elements, dust, and radiation from stars and dust in galaxies. Our solutions reproduce remarkably well a wide variety of observations that were not used as input. These include the integrated background light from galaxy counts from near-ultraviolet to near-infrared wavelengths, the rest-frame optical and near-infrared emissivities at various redshifts from surveys of galaxies, the mid-infrared and far-infrared emissivities of the local universe from the IRAS survey, the mean abundance of heavy elements at various epochs from surveys of damped Lyman-alpha systems, and the global star formation rates at several redshifts from $H\alpha$, mid-infrared, and submillimeter observations. The chemical enrichment history of the intergalactic medium implied by our models is also consistent with the observed mean metal content of the Lyman-alpha forest at high redshifts. We infer that the dust associated with star forming regions is highly inhomogeneous and absorbs a significant fraction of the starlight, with only 41–46% of the total in the extragalactic optical background and the remaining 59–54% reprocessed by dust into the infrared background. The solutions presented here provide an intriguing picture of the cosmic mean history of galaxies over much of the Hubble time. In particular, the process of galaxy formation appears to have undergone an early period of substantial inflow to assemble interstellar gas at $z \gtrsim 3$, a subsequent period of intense star formation and chemical enrichment at $1 \lesssim z \lesssim 3$, and a recent period of decline in the gas content, star formation rate, optical stellar emissivity, and infrared dust emissivity at $z \lesssim 1$.

Subject headings: cosmology: diffuse radiation — galaxies: evolution — quasars: absorption lines — infrared: galaxies

1. INTRODUCTION

In the past few years, galaxies have been observed to redshifts approaching five, when the universe was less than 10% of its present age. A goal of several recent studies has been to determine the average evolution of the stellar and interstellar contents of the entire population of galaxies. Individual galaxies, spanning a wide range of sizes, masses, and morphological types, certainly had different, possibly complicated histories of star formation, gas consumption, and chemical enrichment. Studying the average properties of galaxies has

the virtue of simplicity and is relevant to several important problems, such as the extragalactic background radiation and the chemical enrichment of the intergalactic medium. Quasar absorption-line and optical imaging and redshift surveys of galaxies, when combined with cosmic infrared background measurements, promise to reveal the unbiased global history of star formation in galaxies. This is the main objective of this paper.

Quasar absorption lines have been used for more than a decade to probe the interstellar content of galaxies at high redshifts. The damped $Ly\alpha$ systems, a subset of the absorption-line systems with highest HI column densi-

ties, are of particular interest because they dominate the mass density of neutral gas in the universe and probably represent the progenitors of present-day galaxies (Wolfe et al. 1986), although the exact nature of these objects (i.e., their morphologies, sizes, and space density) is a topic of current speculation and investigation. Surveys of damped Ly α systems along many lines of sight provide information on the mean comoving density of neutral hydrogen and the mean abundances of heavy elements, dust, and molecules at various redshifts. The picture that emerges, while still incomplete, already reveals several important results. First, the damped Ly α systems at $z \approx 3$ contain enough cool, neutral gas to form all of the stars visible today (Wolfe et al. 1995). Second, the observed decrease of the gas content from $z \approx 3$ to $z = 0$ plausibly reflects the conversion of gas into stars (Lanzetta, Wolfe, & Turnshek 1995). Third, the damped Ly α systems at $z \approx 3$ are still in their infancy of chemical enrichment, with low metallicity (Pettini et al. 1994), low dust-to-gas ratio (Pei, Fall, & Bechtold 1991) and few molecules (Levshakov et al. 1992). These observations, when tied together by models of cosmic chemical evolution, predict high rates of star formation at $1 \lesssim z \lesssim 2$ and a rapid decline toward $z = 0$ (Pei & Fall 1995).

Recently, optical imaging and redshift surveys have given us a direct view of the stellar content of the distant universe (Lilly et al. 1995; Steidel et al. 1996; Ellis et al. 1996; Cowie et al. 1996; Williams et al. 1996). An important quantity that can be measured from these surveys is the mean rest-frame ultraviolet emissivity as a function of redshift, which potentially traces the global history of star formation in the universe. The optical data suggest that the average rate of star formation increases with time at $z \gtrsim 2$ (Madau et al. 1996), peaks near $z \approx 1 - 2$ (Connolly et al. 1997), and then declines sharply to $z = 0$ (Lilly et al. 1996), although the apparent increase from $z \approx 4$ to $z \approx 3$ is quite uncertain (Steidel et al. 1999). This picture is broadly consistent with the history of star formation inferred from models of cosmic chemical evolution with input from surveys of damped Ly α systems (Fall 1998). Thus, cosmic chemical evolution provides a key link between the stellar, gaseous, and chemical constituents of galaxies.

All-sky surveys from the DIRBE and FIRAS instruments on the *COBE* satellite have provided us with another view of the integrated emission history of the universe from far-infrared to millimeter wavelengths (Puget et al. 1996; Schlegel, Finkbeiner, & Davis 1998; Hauser et al. 1998; Fixsen et al. 1998). The recent DIRBE and FIRAS detections of the cosmic infrared background, when compared with the Hubble Deep Field survey, indicate that a significant fraction of the radiation released

by stars has not been seen in the ultraviolet and optical region of the extragalactic background, but rather at far-infrared wavelengths (Hauser et al. 1998). The large amount of far-infrared radiation seen by the DIRBE and FIRAS appears to imply that the global star formation rate currently deduced from optical surveys is severely biased (Dwek et al. 1998; Blain et al. 1999; Calzetti & Heckman 1999). This bias is not entirely surprising because galaxies undergoing bursts of star formation are known not only to be sources of intense ultraviolet radiation but also of far-infrared radiation. The cosmic infrared background records the cumulative infrared emission from galaxies at all redshifts and therefore provides an important constraint on the global history of star formation.

In this paper, we combine the available data from quasar absorption-line surveys, optical imaging and redshift surveys, and extragalactic background measurements to derive the cosmic histories of star formation, gas consumption, and chemical enrichment in galaxies. Our approach is an extension of the studies of Pei & Fall (1995) and Fall, Charlot, & Pei (1996). These are based on a set of equations that link the comoving densities of stars, interstellar gas, heavy elements, and dust, averaged over the whole population of galaxies. The data from quasar absorption-line surveys and optical imaging and redshift surveys are taken as inputs, and the effects of dust are self-consistently coupled to the production of heavy elements. A key constraint in the present paper is imposed by the recent DIRBE and FIRAS measurements of the cosmic infrared background. With a self-consistent treatment of the absorption and reradiation of starlight by dust, the problem is then to solve the set of coupled chemical equations so that the reradiated starlight by dust matches the background measurements. Section 2 presents the basic method, states the key assumptions, and identifies the necessary observational inputs. In § 3, we derive the global histories of stars, interstellar gas, heavy elements, dust, radiation from stars and dust, and baryon flow between the interstellar and intergalactic media. In § 4, we discuss the major uncertainties in the models and some of the implications of our results. Our conclusions are summarized in § 5. Throughout the paper, we adopt a cosmology with $\Lambda = 0$, $q_0 = 1/2$, and $H_0 = 50 \text{ km s}^{-1} \text{ Mpc}^{-1}$.

2. MODELS

We are interested in the global evolution of stars, interstellar gas, heavy elements, dust, and radiation from stars and dust, all averaged in comoving volumes large enough to contain many galaxies. The basic formalism that can be used to describe this evolution has been de-

veloped by Lanzetta et al. (1995), Pei & Fall (1995), and Fall et al. (1996). Our previous work showed that the emission history of galaxies could be inferred from their absorption history with the aid of stellar population synthesis models, and that self-consistent solutions of the equations of cosmic chemical evolution predicted high rates of star formation at $1 \lesssim z \lesssim 2$ and declining rates at $0 \lesssim z \lesssim 1$. Here, we adopt nearly the same formalism in describing cosmic chemical evolution but without any assumption about the baryon flow rate between the interstellar and intergalactic media, and develop some new formulae for the absorption and reradiation of starlight by dust. With observations now available on the absorption and emission histories of galaxies, we can use both of these as inputs, while the reradiation of starlight absorbed by dust is constrained by the measured cosmic infrared background radiation. In this way, we obtain the unbiased absorption and emission histories of galaxies as well as the evolution of baryons within galaxies.

2.1. Cosmic Chemical Evolution

The equations of cosmic chemical evolution govern the global rates of star formation, gas consumption, and chemical enrichment. For a population of galaxies, these rates can be expressed most simply in terms of the mean comoving densities of stars, interstellar gas, and elements heavier than He in the interstellar medium, Ω_s , Ω_g , and Ω_m , all measured in units of the present critical density ($\rho_c = 3H_0^2/8\pi G$), and the mean abundance of heavy elements in the interstellar media of galaxies $Z \equiv \Omega_m/\Omega_g$. As defined here, Ω_s , Ω_g , Ω_m , and Z all pertain to galaxies themselves, not to the intergalactic medium. On the timescale of interest here (the Hubble time), any delayed recycling of stellar material to the interstellar medium can be neglected. We can therefore write, in the approximation of instantaneous recycling (and $Z \ll 1$),

$$\dot{\Omega}_g + \dot{\Omega}_s = \dot{\Omega}_f, \quad (1)$$

$$\Omega_g \dot{Z} - y \dot{\Omega}_s = (Z_f - Z) \dot{\Omega}_f, \quad (2)$$

where y is an “effective yield” of heavy elements and the dots denote differentiation with respect to proper time. The source terms on the right-hand sides of equations (1) and (2), with subscript f , represent the inflow or outflow of gas with mean metallicity Z_f at a net comoving rate $\dot{\Omega}_f$ to or from galaxies. These equations can be derived by summing the corresponding equations for the chemical evolution of all the individual galaxies in a large comoving volume (see Tinsley 1980).

The definition of the effective yield requires some care. It could be defined as the mean nucleosynthetic yield of different galaxies weighted by their star formation

rates. In this case, however, equation (2) would only be valid for a population of chemically homogeneous galaxies (i.e., all galaxies at a given redshift have the same metallicity). The reason for this is that the average over galaxies leading to equation (2) contains a residual term due to the metallicity spread of different galaxies, which can simply be absorbed into the definition of y . In this case, equation (2) is also valid for a population of chemically inhomogeneous galaxies. This definition of the effective yield is entirely appropriate in our models, because we regard y as an output parameter fixed by the mean metallicity at the present epoch (see below).

We now consider a simple case of the inflow or outflow of gas between galaxies and their environment. Inflow ($\dot{\Omega}_f \geq 0$) allows for the addition of unprocessed material ($Z_f = 0$) into galaxies from the intergalactic medium, while outflow ($\dot{\Omega}_f < 0$) allows for the removal of processed material ($Z_f = Z$) from galaxies by supernova explosions, galactic winds, collisions, and so forth. Thus, we write

$$Z_f = Z[1 - \theta(\dot{\Omega}_f)], \quad (3)$$

where θ is the unit step function, defined as $\theta(x) = 1$ for $x \geq 0$ and $\theta(x) = 0$ for $x < 0$. If a significant outflow occurs, it can enrich the intergalactic medium with heavy elements. However, since the gas reservoir in the intergalactic medium is sufficiently large, its overall metallicity is likely to remain lower than that of the interstellar medium within galaxies. Therefore, the assumption of only metal-free inflow should remain roughly valid. In principle, there is a possibility that both inflow and outflow could occur at the same time and with the same rate so that the net flow is zero, in which case equation (3) would be invalid. In practice, as long as the net flow is dominated by either inflow or outflow, equation (3) should be a good approximation.

Equations (1) and (2) can be solved by specifying the initial conditions at $t = 0$ or the boundary conditions at the present epoch, $z = 0$. We assume that, at some early time, before galaxies form, there are no stars, interstellar gas, or heavy elements, i.e., $\Omega_s = \Omega_g = \Omega_m = 0$ at $t = 0$. With these initial conditions and equation (3), the solutions to equations (1) and (2) are

$$\Omega_f = \Omega_g + \Omega_s, \quad (4)$$

$$Z = \int_0^t dt' y \frac{\dot{\Omega}_s(t')}{\Omega_g(t')} \exp \left[\int_t^{t'} dt'' \frac{\theta[\dot{\Omega}_f(t'')] \dot{\Omega}_f(t'')}{\Omega_g(t'')} \right]. \quad (5)$$

The formation and early evolution of galaxies naturally requires an initial inflow, $\dot{\Omega}_f > 0$. Any time variation in y is likely to be weaker than that in Ω_s , which varies by more than an order of magnitude over $0 \lesssim z \lesssim 5$. As an approximation, we assume that the effective yield y

is constant in time. Since Z and y always appear in the combination Z/y , we can fix y by imposing a boundary condition on the mean metallicity Z at $z = 0$. The quantity $Z(0)$, which refers to an average over all galaxies at the present epoch, is not known precisely. We simply assume that the metallicity in the solar neighborhood is typical and adopt $Z(0) = Z_\odot$. The values of $Z(0)$ and all other input parameters in our models are listed in Table 1.

Our choice of the initial conditions for Ω_s and Ω_g has a special meaning in the models of cosmic chemical evolution: the quantity Ω_f at any redshift is always the sum of the comoving densities of stars and interstellar gas, and hence represents the comoving density of baryons within galaxies. The evolution of the baryon content in galaxies is regulated by the star formation rate and the gas consumption and inflow or outflow rates. If the star formation rates were relatively small at some early epochs, i.e., $\dot{\Omega}_s \ll \dot{\Omega}_g$, the evolution of galaxies would be dominated by the build up of interstellar gas, i.e., $\dot{\Omega}_f \approx \dot{\Omega}_g$. On the other hand, if the star formation rates were relatively high, this would dominate the evolution. In fact, the process of galaxy formation might proceed through two phases: (1) the accretion of baryons during an early period of gas assembly, and (2) the production of heavy elements and consumption of gas during a subsequent period of star formation.

The total abundance of heavy elements Z in equation (5) includes metals in both the gas and solid phases of the interstellar medium. The production of dust is therefore included naturally in our approach. We assume for simplicity that a fixed fraction of the heavy elements in the interstellar medium is locked up in dust grains. In this case, the comoving density of dust Ω_d is related to the comoving density of heavy elements Ω_m by

$$\Omega_d = d_m \Omega_m = d_m Z \Omega_g, \quad (6)$$

with a constant dust-to-metals mass ratio d_m . In addition to some theoretical expectations for a constant d_m (Dwek 1998), there is also empirical evidence for this in nearby galaxies and the damped Ly α systems at high redshifts. For the Milky Way and the Large and Small Magellanic Clouds, the dust-to-metals ratio is 0.51 (GAL), 0.36 (LMC), and 0.46 (SMC) (Pei 1992; Luck & Lambert 1992), roughly constant even though the dust-to-gas ratios and metallicities in these galaxies vary by nearly an order of magnitude. Using the measurements of the gas-phase depletion of Cr relative to Zn in a sample of damped Ly α systems by Pettini et al. (1997a), we derive mean values $d_m = 0.45$ at $0.7 < z \leq 1.0$, 0.37 at $1.0 < z \leq 2.0$, and 0.44 at $2.0 < z \leq 2.8$, with the assumptions that the intrinsic Cr/Zn is solar, that Cr is depleted onto grains, while Zn is not, and that the

dust has Galactic chemical composition and SMC-type extinction curve. These results are consistent with estimates based on the observed gas-phase depletions of other elements in damped Ly α systems (Kulkarni, Fall, & Truran 1997; Vladilo 1998). Figure 1 shows our estimates of d_m as a function of redshift, where the data point at $z = 0$ is the mean for the Milky Way, LMC, and SMC. Evidently, the mean dust-to-metals ratio is roughly constant at $d_m = 0.45$ over a significant range of redshifts, $0 \leq z \lesssim 3$.

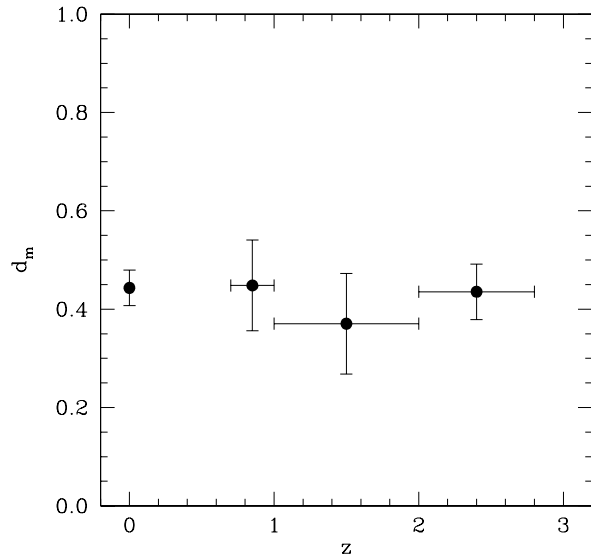


FIG. 1.—Mean dust-to-metals mass ratio d_m as a function of redshift. The data point at $z = 0$ is the mean in the Milky Way, LMC, and SMC (Pei 1992; Luck & Lambert 1992), while the others are derived from measurements of the gas-phase depletion of Cr relative to Zn in damped Ly α systems (Pettini et al. 1997a). The error bars represent 1σ uncertainties in the means.

The equations presented above for cosmic chemical evolution are quite general and can be used to study the main baryonic ingredients of galaxies and their evolution. The global quantities of interest here include the comoving densities of stars (Ω_s), interstellar gas (Ω_g), heavy elements (Ω_m), dust (Ω_d), and baryons (Ω_f) in galaxies, and the comoving rates of star formation ($\dot{\Omega}_s$), gas accretion ($\dot{\Omega}_g$), metal enrichment ($\dot{\Omega}_m$), dust production ($\dot{\Omega}_d$), and baryon flow ($\dot{\Omega}_f$), all as functions of redshift. With equations (4)-(6) and straightforward time differentiation and integration between the comoving density and rate pairs, there are only two (functional) degrees of freedom in the problem, namely, inputs of any two independent quantities as functions of

redshift allow all others to be derived. We choose $\Omega_g(z)$ and $\dot{\Omega}_s(z)$ as the two inputs, since both can be traced over a wide range of redshifts by observations.

2.2. Absorption History

The damped Ly α systems have HI column densities in excess of $2 \times 10^{20} \text{ cm}^{-2}$ and account for more than 80% of the neutral gas in the universe (Lanzetta et al. 1991). The other quasar absorption-line systems, those with HI column densities less than 10^{20} cm^{-2} , probably contain more gas in total than the damped Ly α systems, but this gas is diffuse and highly ionized. The damped Ly α systems are usually interpreted as the ancestors of present-day galaxies, but it is not yet clear whether they are mainly the progenitors of galactic disks or spheroids, or dwarf galaxies. However, the comoving density of HI, the quantity of interest here, can be computed directly from the statistics of the absorption along random lines of sight and is therefore independent of the morphologies, sizes, and other properties of the damped Ly α systems. The main restriction on our results is that they do not include any galaxies that consumed their neutral gas before $z \approx 4$, the highest redshift probed systematically by existing surveys of damped Ly α systems.

2.2.1. Comoving Density of Gas

The interstellar content of galaxies consists mainly of hydrogen and helium (in neutral atomic, ionized, and molecular forms); thus

$$\Omega_g = \mu\Omega_{\text{H}} = \mu(\Omega_{\text{HI}} + \Omega_{\text{HII}} + \Omega_{\text{H}_2}), \quad (7)$$

where μ is the mean particle mass per H atom, and HI, HII, and H₂ denote neutral atomic, ionized, and molecular hydrogen, respectively. The damped Ly α systems are probably mainly neutral, because their HI column density exceeds $N \gtrsim 2 \times 10^{20} \text{ cm}^{-2}$ and their metal absorption lines usually show low ionization states. They also appear to have low abundances of molecules, at least at high redshifts (Levshakov et al. 1992; Ge & Bechtold 1997). As an approximation, we ignore HII and H₂ but include He:

$$\Omega_g = \mu\Omega_{\text{HI}}, \quad (8)$$

with $\mu = 1.3$, appropriate for 23% primordial He by mass from Big Bang nucleosynthesis (Hogan, Oliver, & Scully 1997). While the neglect of H₂ is probably reasonable at high redshifts, it is less accurate toward $z = 0$. In the local universe, the observed H₂ and HI masses of 154 late-type galaxies (Sa to Im) give an averaged H₂-to-HI mass ratio of roughly 0.8, implying 45% of H in H₂ (Young & Scoville 1991). Thus, it appears that equation (8) is approximately valid (to within a factor

of two) over much or all of cosmic history.

The comoving density of HI as a function of redshift is given by

$$\Omega_{\text{HI}}(z) = \frac{8\pi G m_{\text{H}}}{3cH_0} \int_0^\infty dN N f(N, z), \quad (9)$$

where m_{H} is the mass of the H atom, and f is the distribution of HI column densities, defined such that $f(N, z)dNdX$ is the number of absorbers along a random line of sight with HI column densities between N and $N + dN$ and redshift paths between X and $X + dX$ [with $dX = (1+z)(1+2q_0z)^{-1/2}dz$ for $\Lambda = 0$] (Lanzetta et al. 1991). The existing samples of damped Ly α systems are all derived from optically selected quasars. As a result of the obscuration caused by dust within the damped Ly α systems, these samples are biased to some degree (Fall & Pei 1993). Thus, we introduce the observed comoving density of HI

$$\Omega_{\text{HIo}}(z) = \frac{8\pi G m_{\text{H}}}{3cH_0} \int_0^\infty dN N f_o(N, z), \quad (10)$$

where f_o represents the observed distribution of HI column densities in damped Ly α systems. In the limit of an infinitely large sample of absorbers, the true and observed distributions, f and f_o , sample all impact parameters and orientations of galaxies, and the resulting comoving densities, Ω_{HI} and Ω_{HIo} , can be derived without any knowledge of the sizes or shapes of galaxies.

Both Ω_{HI} and Ω_{HIo} are averages over the population of damped Ly α absorbers, but the former pertains to random lines of sight, while the latter pertains to the lines of sight to optically selected quasars. Since the missing absorbers in an optically selected sample tend to be those with the highest N , there can be large differences between Ω_{HI} and Ω_{HIo} and this can affect the resulting picture of cosmic chemical evolution (Pei & Fall 1995). We neglect another potential bias, that due to the magnification of quasars by gravitational lenses associated with foreground damped Ly α systems, because this appears to be a relatively minor effect in the samples from which Ω_{HIo} has been estimated (Le Brun et al. 1997; Perna et al. 1997; Smette et al. 1997). Since the dust-to-gas ratios are not known individually for many damped Ly α systems, the conversion from Ω_{HIo} to Ω_{HI} must be made statistically. For this purpose, we introduce a mean correction factor Q , defined by the relation

$$\Omega_{\text{HI}}(z) = \Omega_{\text{HIo}}(z)Q(z). \quad (11)$$

2.2.2. Missing Absorbers

The relation between the true and observed distributions of HI column densities can be derived under two idealizations: that the absorbers are obtained from a

magnitude limited sample of bright quasars, and that all absorbers at a given redshift have the same dust-to-gas ratio. In this case, we have (Fall & Pei 1993)

$$f(N, z) = f_o(N, z) \exp[\beta\tau(N, z)], \quad (12)$$

$$\tau(N, z) = k_m(z) m_H N \kappa_e [\lambda_e / (1 + z)], \quad (13)$$

$$k_m(z) = \Omega_d(z) / \Omega_{\text{HI}}(z), \quad (14)$$

where β is the power-law index of the bright part of the quasar luminosity function [i.e., $\phi(L, z) \propto L^{-\beta-1}$], τ is the extinction optical depth at $z = 0$, k_m is the mean dust-to-HI mass ratio, κ_e is the mass extinction coefficient evaluated at a wavelength $\lambda = \lambda_e / (1 + z)$, and λ_e is the effective wavelength of the limiting magnitude. Equations (12)-(14) are also valid for combinations of samples with different limiting magnitudes, provided these are brighter than $V \lesssim 20$, and they are good approximations when there is a dispersion in the dust-to-HI ratio, provided this satisfies $\sigma(\log k_m) \lesssim 1$. Both conditions appear to be true for the existing samples of damped Ly α systems and background quasars (see § 2.2.3 and § 2.2.4).

To derive the correction factor Q , we must adopt a specific form for the observed distribution of HI column densities. A common approximation is a power law, $f_o(N, z) \propto N^{-\gamma}$, with $\gamma \approx 1.7$ (Lanzetta et al. 1991). Unfortunately, this gives a divergent total mass in equation (10), unless an upper cutoff in N is imposed. Thus, following Pei & Fall (1995), we adopt the gamma distribution

$$f_o(N, z) = (f_*/N_*) (N/N_*)^{-\gamma} \exp(-N/N_*), \quad (15)$$

where f_* and N_* specify the normalization and “knee” of the function. This parametric form provides a solution to the problem of diverging mass and a better fit to the data than the power-law form (Storrie-Lombardi et al. 1996a). In this case, the true distribution f from equation (12) is also a gamma distribution

$$f(N, z) = (f_t/N_t) (N/N_t)^{-\gamma} \exp(-N/N_t), \quad (16)$$

with $f_t = Q^{\frac{\gamma-1}{\gamma-2}} f_*$ and $N_t = Q^{\frac{1}{2-\gamma}} N_*$. For $\gamma < 2$, the observed and true comoving densities of HI are simply $\Omega_{\text{HI}o} = (8\pi G m_H / 3cH_0) \Gamma(2 - \gamma) f_* N_*$ and $\Omega_{\text{HI}} = (8\pi G m_H / 3cH_0) \Gamma(2 - \gamma) f_t N_t$. Combining equations (9)-(15) and eliminating N_* in favor of γ and f_* , we obtain

$$Q = \beta\tau_* + Q^{\frac{\gamma-1}{\gamma-2}}, \quad (17)$$

$$\tau_*(\lambda_e, z) \equiv \frac{3cH_0}{8\pi G f_* \Gamma(2 - \gamma)} \Omega_d(z) \kappa_e [\lambda_e / (1 + z)], \quad (18)$$

where Γ denotes the standard gamma function. Equation (17) is an implicit relation from which Q can be obtained as a function of $\beta\tau_*$ and γ . For $\gamma = 1$, we have $Q = 1 + \beta\tau_*$ and, for $\gamma = 3/2$, we have $Q =$

$$[1 + (\beta\tau_*/2)^2]^{1/2} + (\beta\tau_*/2).$$

2.2.3. Inputs from Damped Ly α Surveys

The formulae presented above enable us to compute the true Ω_g from the observed comoving density of HI, $\Omega_{\text{HI}o}$. This relation is

$$\Omega_g(z) = \mu \Omega_{\text{HI}o}(z) Q(z), \quad (19)$$

where μ accounts for He and Q accounts for the missing damped Ly α systems in an optically selected sample of quasars. The correction factor Q depends on the mean comoving density of dust Ω_d , the extinction coefficient of grains κ_e , the bright-end slope of the quasar luminosity function β , the effective wavelength of the quasar sample λ_e , the slope of the absorber column density distribution γ , and the characteristic sky coverage of the absorbers f_* . Because Q is linked to Ω_d , our solutions of the equations of cosmic chemical evolution are obtained iteratively (see § 3). In the following, we adopt $\Omega_{\text{HI}o}(z)$ at various redshifts from surveys of the damped Ly α systems and estimate the values of the parameters ($\beta, \lambda_e, \gamma, f_*$) appropriate for these surveys.

The observed HI content in the damped Ly α systems has been traced over the range of redshift $0.008 \leq z \leq 4.7$, in surveys by Wolfe et al. (1986, 1995), Lanzetta et al. (1991, 1995), and Storrie-Lombardi et al. (1996b). We adopt the most recent determinations of $\Omega_{\text{HI}o}(z)$, derived by Storrie-Lombardi et al. (1996b) assuming a particular cosmology with $\Lambda = 0$, $q_0 = 1/2$, and $H_0 = 50 \text{ km s}^{-1} \text{ Mpc}^{-1}$. These estimates, listed in Table 2 with their errors, are based on 44 damped Ly α systems obtained from a combined sample of 366 optically selected quasars. The statistical uncertainty in $\Omega_{\text{HI}o}(z)$ is roughly 50%. The present value $\Omega_{\text{HI}o}(0)$ is not directly determined from absorption in damped Ly α systems, and, as a result, is not available as input to our models. Instead, we appeal to observations of 21 cm emission for the HI content of galaxies in the local universe (§ 2.2.6).

The existing samples of damped Ly α systems have been obtained from samples of quasars selected by $V \leq 18.5$ (Wolfe et al. 1986; Lanzetta et al. 1991), $B \leq 18.75$ (Wolfe et al. 1995), $V \lesssim 17$ (Lanzetta et al. 1995), and $R \leq 19.5$ (Storrie-Lombardi et al. 1996a). Thus, they do not conform to the idealization of a single limiting magnitude under which equation (12) was derived. Fortunately, all of the samples are brighter than $V \approx 20$. In this case, the luminosity function of quasars is well approximated by a single power law (Hartwick & Schade 1990; Pei 1995). The limiting magnitudes cancel out and do not appear explicitly in equation (12), except through the effective wavelength λ_e . Therefore, our formulae for Q are also valid for combinations of samples with different limiting magnitudes. The value

of β can be determined most simply from the differential counts $A(m)$ of quasars versus apparent magnitude m , because $\phi(L, z) \propto L^{-\beta-1}$ implies $A(m) \propto 10^{0.4\beta m}$. Figure 2 shows the observed B -band counts from Hartwick & Schade (1990). The line is a weighted, least-squares fit to the data at $B \leq 20$, with the χ^2 -fitted value of β listed in Table 1. At $z < 3.5$, most of the absorbers come from the V -selected quasars, while at $z \geq 3.5$, all of them come from the R -selected quasars. Accordingly, we adopt $\lambda_e = 5500 \text{ \AA}$ at $z < 3.5$ and $\lambda_e = 6500 \text{ \AA}$ at $z > 3.5$. The value of λ_e at $z = 0$ does not enter our calculations but implies a specific value of $\Omega_{\text{HIo}}(0)$ for the purpose of comparison (§ 2.2.6).

The current data for the observed distribution f_o in the damped Ly α systems are sparse but nevertheless indicate that the evolution of f_o is strongest for the high- N systems (Wolfe et al. 1995; Storrie-Lombardi et al. 1996a). In the gamma distribution model, this is equivalent to varying N_* with respect to z , and hence the evolution of Ω_{HIo} is predominantly due to N_* rather than γ and f_* . Thus, it is a good approximation to regard γ and f_* as constants. We determine these parameters by fitting the cumulative form of f_o , i.e., the observed number $n_o(>N)$ of absorbers with HI column densities greater than N . The results are shown in Figure 3, where the data (in the stepped line and the circle) are

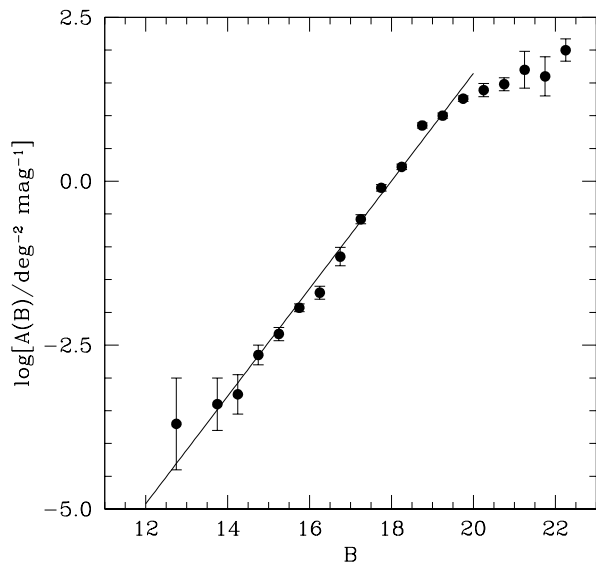


FIG. 2.—Differential counts of quasars per square degree versus B magnitude. The data points were derived by Hartwick & Schade (1990) from a combined sample of more than 1000 quasars over $0 \leq z \leq 3.3$. The line is a weighted, least-squares fit to the observations at $B \leq 20$, relevant to the samples of quasars from which the damped Ly α systems were selected.

from Storrie-Lombardi et al. (1996a). The curve is the gamma distribution (integrated over the redshift path of all absorbers in the sample), with the fitted values of γ and f_* listed in Table 1. The circle at $N = 1.6 \times 10^{17} \text{ cm}^{-2}$ is the number of Lyman-limit systems that would be detected along the same redshift path as in the damped Ly α sample. We have included it in our fits to reduce further the uncertainty in γ and f_* , especially the former. The values of γ and f_* derived here are similar to those obtained by Storrie-Lombardi et al. (1996a) from a maximum likelihood fit.

2.2.4. Dispersion in the Dust-to-Gas Ratio

The main idealization in our derivation of the mean correction Q is the assumption that all absorbers at a given redshift have the same dust-to-gas ratio. This gives a simple relation between the true and observed distributions in equation (12) so that Q can be evaluated using f_o (or f). It also links the dust-to-HI ratio k_m to the comoving density of dust in equation (14) so that Q is coupled self-consistently to the equations of chemical evolution. The damped Ly α systems do show a significant dispersion in their dust-to-gas ratios, as indicated by the observed Cr/Zn ratios (Pettini et al. 1997a). A dispersion in the dust-to-gas ratio would

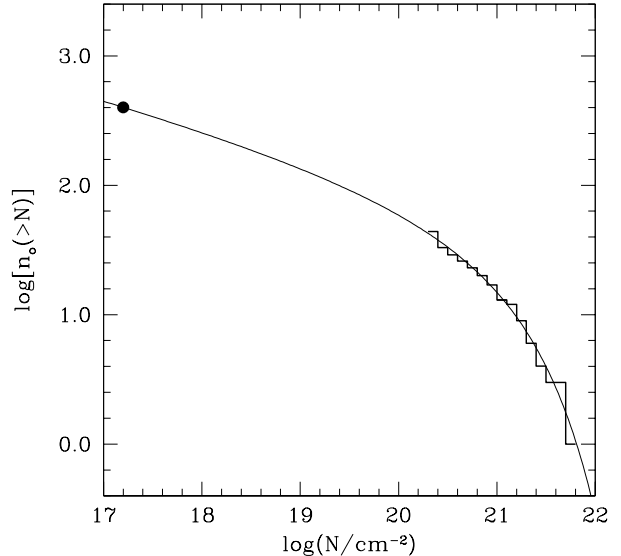


FIG. 3.—Cumulative number of absorption systems with HI column densities greater than N . The stepped line represents the data from existing surveys of damped Ly α systems (with a total redshift path $\Delta X = 421$), while the point is the mean number of Lyman limit systems that would be detected along the same redshift path (Storrie-Lombardi et al. 1996b). The curve shows the fit of the cumulative form of the gamma distribution.

introduce additional terms of N in the relation between f and f_o , rather than the simple relation in equation (12) (see the Appendix of Fall & Pei 1993). Nearby galaxies have $\sigma(\log k_m) \approx 0.4 - 0.5$ (Pei 1992) and the observed damped Ly α systems have $\sigma(\log k_m) \approx 0.6$ at $0.7 < z < 2$ and 0.6 at $2 < z < 2.8$ (Pettini et al. 1997a). If the true dispersion were not much larger than the observed one, the additional terms in the relation between f and f_o would be negligible (less than roughly 20% at $N = 10^{21} \text{ cm}^{-2}$ for $k_m = 0.1 Z_\odot$). Thus, the mean correction Q derived here is not sensitive to a modest dispersion in the dust-to-gas ratio [i.e., $\sigma(\log k_m) \lesssim 1$].

A dispersion in the dust-to-gas ratio could, however, affect the observed mean dust-to-gas ratio and metallicity in damped Ly α absorbers. The observed mean dust-to-gas ratio could be underestimated, because the absorbers with highest dust-to-gas ratios at fixed HI column density would be preferentially missing from optically selected quasars. Using the formulae of Fall & Pei (1993), we estimate that the observed mean dust-to-gas ratio would be 30% – 50% lower than the true mean for $\sigma(\log k_m) \approx 0.4 - 0.6$ (at $k_m = 0.1 Z_\odot$). If the heavy elements in individual galaxies were correlated with the dust, the observed mean metallicity would also be underestimated by a similar amount. These biases, while not negligible, are comparable to the observational uncertainties in the derived mean dust-to-gas ratios and metallicities in the current samples of damped Ly α systems. We emphasize that our models of cosmic chemical evolution do not use as input the observed comoving densities of dust and metals, and consequently they are not affected by a dispersion in the dust-to-gas ratio. The only complication is that, since no corrections are made, this could affect the comparison of our model outputs with the observed mean dust-to-gas ratio and metallicity in the damped Ly α systems.

2.2.5. Optical Properties of Grains

The optical properties of interstellar dust grains at high redshifts are largely unknown. We must therefore appeal to the properties of galaxies at the present epoch. The Milky Way, LMC, and SMC are three nearby galaxies with well observed interstellar extinction curves. To derive self-consistently the wavelength dependence of the albedo (relevant for the absorption of starlight by dust discussed in § 2.3), we adopt the Draine & Lee (1984) grain model but with the proportions of graphite and silicates adjusted so as to fit the mean empirical extinction curves in the Milky Way, LMC, and SMC (Pei 1992). Figure 4 shows the resulting opacities, κ_e (mass extinction coefficient in the upper panel) and κ_a (mass absorption coefficient in the lower panel), as functions of wavelength in the three galaxies. The range in κ_e be-

tween the Milky Way, LMC, and SMC is roughly 30%, whereas the range in κ_a can be as large as a factor of two, especially at optical wavelengths. The LMC and SMC have lower abundances of metals and dust than the Milky Way and may be more representative of galaxies at high redshifts. There is some evidence for this from the weak or absent 2200 Å “absorption” feature in the damped Ly α systems (Pei et al. 1991). In our calculations, we adopt the LMC-type dust, representing an intermediate case between the Galactic-type and SMC-type dust. We will later discuss the effects of different κ_a on our results (§ 4.2).

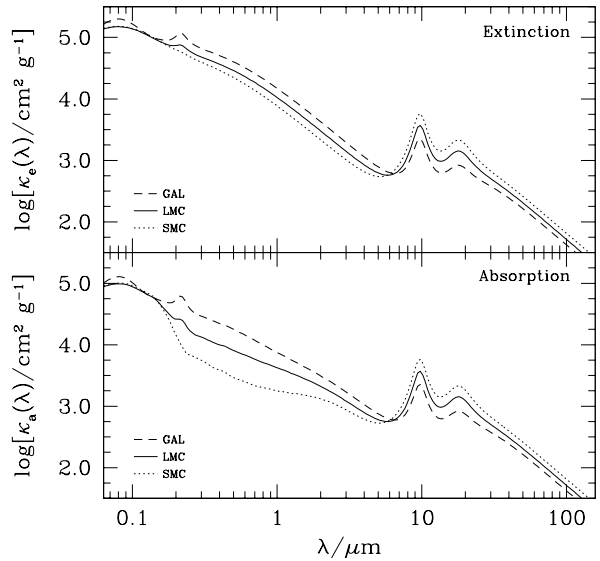


FIG. 4.—Extinction and absorption coefficients (per unit mass) of grains in the Milky Way, LMC, and SMC. These are based on the Draine & Lee (1984) model but with the proportions of graphite and silicates adjusted to fit the observed mean extinction curves in the three galaxies (Pei 1992).

2.2.6. Neutral Gas in the Local Universe

The existing samples of damped Ly α systems contain only a few absorbers at $z \lesssim 2$, causing nearly 60% uncertainty in the corresponding estimates of $\Omega_{\text{HIo}}(z)$ in Table 2. The value of Ω_{HIo} at $z = 0$, if extrapolated from these entries, is even more uncertain. To minimize this uncertainty, we note that averages over the HI content of galaxies in the local universe give $\Omega_{\text{HI}}(0) = (3.8 \pm 0.9) \times 10^{-4}$ (Fall & Pei 1993; Rao & Briggs 1993; Zwaan et al. 1997). This estimate of $\Omega_{\text{HI}}(0)$ is based on 21 cm emission from galaxies, and unlike $\Omega_{\text{HIo}}(0)$, it is not affected by dust obscuration. Thus, we adopt this to fix the present true comoving density of gas in our models, listed in Table 2 as the

first entry under $\Omega_g(z)$. Galaxies at $z = 0$ contain dust and hence cause some difference between $\Omega_{\text{HI}}(0)$ and $\Omega_{\text{HIo}}(0)$. The value of $\Omega_{\text{HI}}(0)$ adopted here implies $\Omega_{\text{HIo}}(0) = (2.2 - 2.7) \times 10^{-4}$ in our models, consistent with the range of $\Omega_{\text{HIo}}(0) = (2.1 - 3.0) \times 10^{-4}$ that would be extrapolated from the data in the damped Ly α systems [with a form $\log \Omega_{\text{HIo}}(z) \propto z$ or $\log \Omega_{\text{HIo}}(z) \propto \log(1+z)$ at $z \lesssim 2$].

2.3. Emission History

We now turn to the second input to our models, $\dot{\Omega}_s(z)$. Deep optical imaging surveys probe the rest-frame ultraviolet radiation of high-redshift galaxies and the rest-frame optical radiation of low-redshift galaxies. When combined with redshift estimates, they trace the stellar emission history of galaxies. The ultraviolet light is produced mainly by short-lived, massive (O and early B) stars and can be used to infer the instantaneous star formation rate, nearly independent of the prior star formation history. However, ultraviolet radiation may be strongly absorbed by dust, and the star formation rate may be severely underestimated if no corrections are made. Since the absorbed starlight is reradiated by dust, the recent measurements of the cosmic infrared background by the DIRBE and FIRAS provide a crucial constraint, which allows us to correct for any radiative energy that is missing in the optical data. The infrared background is the cumulative result of emission at all redshifts. When combined with the chemical equations, the redshift information is then decoded from the integrated background constraint. This section provides a self-consistent treatment of the absorption and reradiation by dust in order to obtain unbiased estimates of the global rates of star formation.

2.3.1. Emissivity and Background Intensity

We are interested in the global evolution of the radiation from stars and dust in galaxies. This evolution can be described naturally in terms of the comoving emissivity $E_\nu(z)$ as a function of redshift, defined here as the power radiated per unit frequency per unit comoving volume at the redshift z . When computing E_ν , we include only photons that have escaped from galaxies and neglect the absorption of infrared photons. This emissivity is then a sum of the direct (but attenuated) starlight and the reradiated starlight from dust in galaxies:

$$E_\nu = (1 - A_\nu)E_{s\nu} + E_{d\nu}, \quad (20)$$

where A_ν is the mean fraction of photons absorbed by dust in the interstellar medium, and $E_{s\nu}$ and $E_{d\nu}$ are the stellar and dust emissivities, respectively. It is clear that $E_{s\nu}$ dominates at ultraviolet, optical, and near-infrared

wavelengths, while $E_{d\nu}$ dominates at mid-infrared, far-infrared, and submillimeter wavelengths. The cosmic background intensity J_ν at $z = 0$, defined as the power received per unit frequency per unit area of detector per unit solid angle of sky, is given by an integral of $E_\nu(z)$ over z :

$$J_\nu = \frac{c}{4\pi} \int_0^\infty dz E_\nu(1+z) \left| \frac{dt}{dz} \right|. \quad (21)$$

We have ignored any external absorption along the line of sight between the sources of radiation and the observer, because all ionizing photons are assumed to be absorbed locally within the galaxies in which they were produced, and because relatively few non-ionizing photons are absorbed by the dust in intervening galaxies. We have checked that, when external absorption by dust is included in our models, only 3% of the observed V-band radiation is absorbed along the line of sight from $z = 5$ to $z = 0$.

2.3.2. Stellar Emissivity

The intrinsic stellar emissivity (before absorption) can be expressed in terms of the comoving rate of star formation $\dot{\Omega}_*$:

$$E_{s\nu} = \rho_c \int_0^t dt' F_\nu(t - t') \dot{\Omega}_*(t'), \quad (22)$$

where $F_\nu(\Delta t)$ is the stellar population spectrum, defined as the power radiated per unit frequency per unit initial mass by a generation of stars with an age Δt . The total rate of star formation $\dot{\Omega}_*$ differs from the net rate $\dot{\Omega}_s$ introduced in § 2.1 because some of the stellar material is ejected back to the interstellar medium by evolving and dying stars; thus

$$\dot{\Omega}_* = (1 - R)^{-1} \dot{\Omega}_s, \quad (23)$$

where R is the IMF-averaged returned fraction. The observed stellar emissivity (after absorption), denoted by $E_{\nu o}$, is then given by

$$E_{\nu o} \equiv (1 - A_\nu)E_{s\nu} = (1 - A_\nu)C_\nu \dot{\Omega}_s, \quad (24)$$

where

$$C_\nu \equiv \frac{\rho_c}{\dot{\Omega}_s(t)} \int_0^t dt' F_\nu(t - t') \frac{\dot{\Omega}_s(t')}{1 - R(t')} \quad (25)$$

is a conversion factor between the intrinsic stellar emissivity and star formation rate, which depends in general on the past history of $\dot{\Omega}_s$. At ultraviolet wavelengths, however, C_ν remains roughly constant in time, nearly independent of the past history of $\dot{\Omega}_s$, and hence $E_{\nu o}(z)$ scales directly with $\dot{\Omega}_s(z)$ in the absence of dust absorption.

We adopt the latest version of the Bruzual-Charlot population synthesis code to compute F_ν and R (Bruzual & Charlot 1998). The stellar IMF is assumed to be a

power law, $\phi(m) \propto m^{-(1+x)}$, with $x = 1.35$ (a Salpeter IMF) and lower and upper mass cutoffs at $0.1 M_\odot$ and $100 M_\odot$. We further assume that all hydrogen ionizing photons are absorbed locally in the interstellar medium, where 68% of them are converted to Ly α photons (the fraction appropriate for case B recombination in gas at 10^4 K). The Ly α photons are assumed to be absorbed by dust (as a result of resonant scattering by HI), and the remaining energy is radiated uniformly in wavelength between 3000 and 7000 Å (a range that includes most of the relevant emission lines). This treatment of ionizing radiation is consistent with ultraviolet observations of local starburst galaxies (Leitherer et al. 1995). In our calculations, templates of F_ν and R are pre-computed for metallicities $Z/Z_\odot = 2.5, 1.0, 0.4, 0.2$, and 0.02 . The metallicity dependence of the spectral evolution is included self-consistently by interpolating the templates according to the solution for Z in our models of cosmic chemical evolution. Examples of these templates are shown in Figure 5. We will later discuss the effects of changes in IMF on our results (§ 4.2).

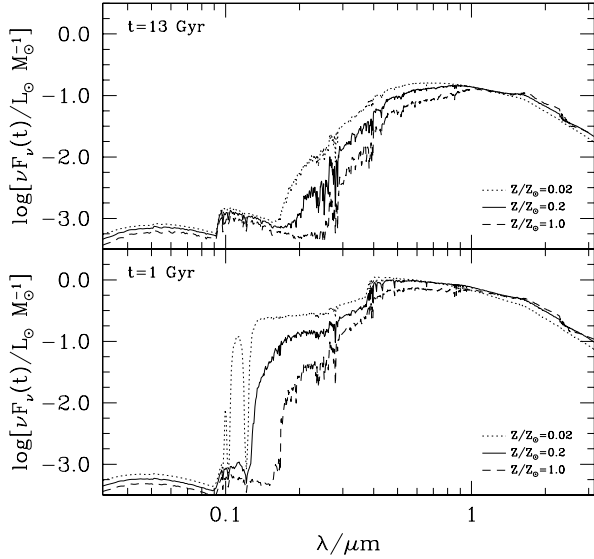


FIG. 5.—Spectra of stellar populations with different ages and metallicities. These are from the latest version of the Bruzual-Charlot (1998) population synthesis code with a Salpeter IMF truncated at 0.1 and $100 M_\odot$.

2.3.3. Absorption of Starlight by Dust

We now consider the mean fraction A_ν of photons absorbed by the interstellar dust in galaxies. This absorption is likely to occur on various scales of the dust distribution, ranging from small clumps of dust shrouding or in the vicinity of individual stars to large clouds in the interstellar medium. To account for all scales, it

is appropriate first to consider the absorption along a ray passing through a galaxy and then to average over all galaxies and all impact parameters and inclination angles to derive the mean absorption. Along such a ray with fixed absorption optical depth τ_ν , the emerging intensity is given by

$$I_\nu(\tau_\nu) = \int_0^{\tau_\nu} d\tau'_\nu S_\nu(\tau'_\nu) \exp[-(\tau_\nu - \tau'_\nu)], \quad (26)$$

where S_ν is the source function along the ray. In the absence of absorption, the corresponding intensity would be

$$I_\nu^0(\tau_\nu) = \int_0^{\tau_\nu} d\tau'_\nu S_\nu(\tau'_\nu). \quad (27)$$

We have ignored the influence of scattering on absorption so that S_ν does not contain a contribution from I_ν . To perform the average over galaxies, we define $g(\tau_\nu, z)d\tau_\nu dX$ as the number of galaxies along a random ray with optical depths between τ_ν and $\tau_\nu + d\tau_\nu$ and redshift paths between X and $X + dX$ when all galaxies and all positions and directions within them are considered. The redshift path, defined by $dX = (1+z)(1+2q_0z)^{-1/2}$ for $\Lambda = 0$, is included in the definition of $g(\tau_\nu, z)$ so that an integral of $\tau_\nu g(\tau_\nu, z)$ over all τ_ν gives the comoving density of dust Ω_d (see eq. 36). With this definition, we can express the mean fraction of photons absorbed by dust in the form

$$A_\nu(z) = \frac{\int_0^\infty d\tau_\nu g(\tau_\nu, z) [I_\nu^0(\tau_\nu) - I_\nu(\tau_\nu)]}{\int_0^\infty d\tau_\nu g(\tau_\nu, z) I_\nu^0(\tau_\nu)}. \quad (28)$$

The distribution function $g(\tau_\nu, z)$ could in principle be modeled by specifying in detail the three-dimensional dust distribution in galaxies of different types, sizes, etc. This would, however, require a large number of assumptions. Instead, we appeal to damped Ly α surveys to specify $g(\tau_\nu, z)$ as a function of both τ_ν and z . In the limit of infinitely many lines of sight, these surveys sample correctly all impact parameters and inclination angles of galaxies at different redshifts. However, the lines of sight in quasar absorption-line surveys have finite resolution, due to the “beam size” of quasar emission regions. Although the exact sizes of quasar emission regions are uncertain, the optical and X-ray continuum regions are often assumed to be much smaller than $0.1 - 1$ pc, which is roughly the size of the broad-line emission region. Thus, even in the limit of infinitely many lines of sight, the resulting distribution function from damped Ly α surveys would not fully sample any small-scale clumpiness of the dust distribution, probably on scales much less than 1 pc but certainly on scales of clumps in the vicinity of individual stars (including circumstellar dust). This distribution, denoted by $h(\tau_\nu, z)$, has the same definition as $g(\tau_\nu, z)$, except that the for-

mer is an unsmoothed version of the latter.

The relation between g and h can be written as

$$g(\tau'_\nu, z) = \int_0^\infty d\tau_\nu p(\tau'_\nu|\tau_\nu) h(\tau_\nu, z), \quad (29)$$

where $p(\tau'_\nu|\tau_\nu)d\tau'_\nu$ is the probability of finding dust clumps with optical depths between τ'_ν and $\tau'_\nu + d\tau'_\nu$ within a small but finite beam given that the beam has a mean optical depth τ_ν . Clearly, this conditional probability must satisfy the following relations

$$\int_0^\infty d\tau'_\nu p(\tau'_\nu|\tau_\nu) = 1, \quad (30)$$

$$\int_0^\infty d\tau'_\nu \tau'_\nu p(\tau'_\nu|\tau_\nu) = \tau_\nu. \quad (31)$$

If the small-scale clumpiness of the dust distribution within galaxies were ignored, i.e., $p(\tau'_\nu|\tau_\nu) = \delta(\tau'_\nu - \tau_\nu)$, we would have $g(\tau'_\nu, z) = h(\tau'_\nu, z)$. Thus, the probability distribution p introduces the additional small-scale clumpiness of the dust distribution specified by g but not sampled by h .

We relate the distribution h of optical depths to the distribution f of HI column densities in the damped Ly α systems (Fall et al. 1996). The absorption optical depth τ_ν and HI column density N are related by

$$\tau_\nu = k_m m_{\text{H}} N \kappa_a(\nu), \quad (32)$$

where κ_a is the mass absorption coefficient of grains and k_m is the dust-to-HI mass ratio (eq. 14). Again, we assume that k_m is only a function of redshift (see § 2.2.2 and § 2.2.4), so that the distributions of τ_ν and N are simply related by $h(\tau_\nu, z)d\tau_\nu = f(N, z)dN$. From equation (16), we then obtain

$$h(\tau_\nu, z) = (f_t/\tau_t)(\tau_\nu/\tau_t)^{-\gamma} \exp(-\tau_\nu/\tau_t), \quad (33)$$

$$\tau_t(\nu, z) \equiv [3cH_0/8\pi G f_t \Gamma(2 - \gamma)] \Omega_d(z) \kappa_a(\nu), \quad (34)$$

where τ_t is the characteristic optical depth of the absorbers. Given the comoving density of dust Ω_d , the absorption opacity of grains κ_a , and the parameters f_t (closely related to f_*) and γ discussed in § 2.2.4, the distribution function h is completely specified by equations (33) and (34). It is known that the distribution of gas in the interstellar medium is not a perfect tracer of the dust distribution, especially on small scales. In this case, the distribution function h , when related to f by a constant k_m , would also undersample some of the small-scale clumpiness of the dust in galaxies.

The probability distribution p specifies the small-scale clumpiness of dust in the interstellar medium. The dust could be in a variety of forms (e.g., shells, spheres, and other complicated shapes) and in a variety of places (e.g., surrounding, in the vicinity of, and between stars). In-

stead of specifying the geometry and location of such clumps relative to the sources of radiation, we adopt a statistical approach to derive p . Since we are interested in the mean quantity A_ν in galaxies, we assume as an idealization that all clumps at a given redshift have the same optical depth τ_c (but not necessarily the same densities, shapes, and sizes), and that such clumps are randomly distributed within the interstellar medium. The probability of intercepting such clumps in a small but finite beam passing through galaxies with a given mean optical depth τ_ν is then given by the usual Poisson distribution:

$$p(\tau'_\nu|\tau_\nu) = \sum_{n=0}^{\infty} \frac{1}{n!} (\tau_\nu/\tau_c)^n \exp(-\tau_\nu/\tau_c) \delta(\tau'_\nu - n\tau_c). \quad (35)$$

This is similar to the clump model developed by Nata & Panagia (1984). It is easy to check that this probability distribution satisfies equations (30)-(31) and that the small-scale clumpiness of dust introduced by p does not affect the total amount of dust, i.e.,

$$\begin{aligned} \Omega_d(z) &= \frac{8\pi G}{3cH_0\kappa_a} \int_0^\infty d\tau_\nu \tau_\nu g(\tau_\nu, z) \\ &= \frac{8\pi G}{3cH_0\kappa_a} \int_0^\infty d\tau_\nu \tau_\nu h(\tau_\nu, z). \end{aligned} \quad (36)$$

Thus, regardless of how clumpy the dust is, the mean comoving density of dust Ω_d computed from h is the same as the one computed from g . This is important because the mean correction factor Q derived in § 2.2.2 is also the same regardless of whether h or g is used.

To derive the mean fraction of photons absorbed by dust A_ν , we further assume that the source function S_ν is constant. Combining equations (28), (29), and (33)-(35), we obtain

$$A_\nu = 1 - \frac{1}{(\gamma - 1)\tau_t} \left\{ \left[1 + \frac{\tau_t}{\tau_c} (1 - e^{-\tau_c}) \right]^{\gamma-1} - 1 \right\}. \quad (37)$$

For $\tau_c = 0$ and $\gamma = 1$, this reduces to the formula derived by Fall et al. (1996). In our new formula, the absorption of starlight by dust depends on the comoving density of dust Ω_d through τ_t and the small-scale clumpiness of the dust through τ_c . The dependence of A_ν on τ_t arises from the absorption of photons traveling through the whole interstellar medium when small-scale dust clumps are unresolved, while the dependence on τ_c includes the additional absorption by such clumps. In the limit of $\tau_t \gg \tau_c$, the absorption is dominated by the dust distribution on scales resolved by quasar absorption-line surveys, whereas, in the limit of $\tau_t \ll \tau_c$, the absorption is dominated by the small-scale clumpiness of the dust. For fixed values of τ_t and τ_c , A_ν depends only mildly on the assumption of a constant source function. For example, for fixed $\tau_t = 0.1$ (1.0) and $\tau_c = 0$, A_ν increases by

1.4% (8%) if the sources are all in the middle of the dust (e.g., stars embedded in clumps) and decreases by 2.6% (17%) if the dust is in the middle of the sources (e.g., clumps between stars), both relative to a constant S_ν . Therefore, the assumption of a constant source function is made here for simplicity and should have only a minor effect on A_ν .

The parameter τ_c is by definition an absorption optical depth, and hence its dependence on frequency is through the absorption coefficient κ_a . It may also have some dependence on redshift as a result of the chemical enrichment and other processes within galaxies. To allow for a range of possibilities, we parameterize this evolution by

$$\tau_c(\nu, z) = \tau_{cV}(0) \left[\frac{\kappa_a(\nu)}{\kappa_a(V)} \right] \left[\frac{\Omega_d(z)}{\Omega_d(0)} \right]^\epsilon, \quad (38)$$

where $\tau_{cV}(0)$ is the visual optical depth of dust clumps at $z = 0$ and ϵ is the power-law index that links τ_c to Ω_d . For $\epsilon = 1$, τ_c would evolve with redshift the same as Ω_d . This might be the case if the metals ejected by stars (including those locked into dust grains) were instantaneously mixed in the interstellar medium, so that τ_c tracked the global chemical enrichment in galaxies. For $\epsilon = 0$, τ_c would remain constant in time. This might be the case if the timescale for mixing were longer than the Hubble time, so that most of the metals remained in the vicinity of stars with little or no evolution. Given these arguments, one might expect that a plausible value of ϵ is somewhere between the cases of instantaneous mixing ($\epsilon = 1$) and the incomplete mixing ($\epsilon = 0$). We treat both τ_{cV} and ϵ as adjustable parameters in our models.

2.3.4. Dust Emissivity

The stellar radiation absorbed by dust is reradiated thermally in the infrared. This emission covers a wide range of wavelengths, reflecting a wide range of grain temperatures. The far-infrared emission is dominated by large amounts of cold dust heated by a smooth field of radiation from many stars. The mid-infrared emission is likely dominated by small amounts of warm and hot dust near stars, including polycyclic aromatic hydrocarbons or very small grains producing some non-equilibrium emission. We write the dust emissivity as a sum of thermal emission at different temperatures:

$$\begin{aligned} E_{d\nu} &= 4\pi\rho_c\Omega_d\kappa_a(\nu) \int_0^\infty dT B_\nu(T)\eta(T) \\ &= 4\pi\rho_c\Omega_d\kappa_a(\nu)\langle B_\nu \rangle, \end{aligned} \quad (39)$$

where $\eta(T)dT$ is the fraction of grains with temperatures between T and $T + dT$ and $\langle B_\nu \rangle$ denotes the average of blackbodies $B_\nu(T)$ over the temperature distribution $\eta(T)$. If all grains had the same temperature T_d , i.e.,

$\eta(T) = \delta(T - T_d)$, $\langle B_\nu \rangle$ would reduce to the spectrum of a single blackbody. The temperature distribution η introduces the warm and hot components of the interstellar dust to account for the mid-infrared emission.

The exact form of the dust temperature distribution is unknown. To specify it fully would require some detailed assumptions about variations of the radiation field, grain spatial density, and optical properties (including the size distribution and the grain composition) throughout galaxies. Since we are more interested in the far-infrared background, where accurate measurements exist, and less interested in the mid-infrared background, where only observational limits exist, we model the dust temperature distribution simply by a power law

$$\eta(T) = \frac{\alpha - 1}{T_c} \left(\frac{T}{T_c} \right)^{-\alpha} \theta(T - T_c). \quad (40)$$

Here, the proportionality is fixed by the requirement that η must be normalized to unity. We have included a truncation factor $\theta(T - T_c)$ to exclude $T < T_c$, because all grains, even those far from stars, will be heated to finite temperatures by the diffuse radiation field of the whole stellar population (or by the cosmic microwave background radiation if this exceeds the diffuse starlight in galaxies). Since the total emission must be finite, the dust temperature index in equation (40) must satisfy $\alpha > 5 + n$ for $\kappa_a(\nu) \propto \nu^n$. Indeed, the observed mean infrared colors of nearby galaxies can be fitted with a value of α that satisfies this requirement (§ 2.3.5). For simplicity, we have not imposed any upper cutoff temperature on η , since this has little effect on our results when α is large. Such a steep slope is the consequence of a very small fraction of mass in warm and hot dust in the interstellar medium.

The lower cutoff temperature T_c in equation (40) is closely related to a mean temperature of dust T_d , defined here by the first moment of T over $\eta(T)$:

$$T_d \equiv \int_0^\infty dT T \eta(T) = \left(\frac{\alpha - 1}{\alpha - 2} \right) T_c. \quad (41)$$

Given the dust temperature index α , the averaged blackbody spectrum $\langle B_\nu \rangle$ is then a unique function of the mean dust temperature T_d . We determine the redshift dependence of this mean temperature by the usual condition of energy balance

$$\begin{aligned} 4\pi\rho_c\Omega_d \int_0^\infty d\nu \kappa_a(\nu) [\langle B_\nu \rangle(T_d) - B_\nu(T_{\text{CMB}})] \\ = \int_0^\infty d\nu A_\nu E_{s\nu}, \end{aligned} \quad (42)$$

where $T_{\text{CMB}} = 2.728(1 + z)$ K is the temperature of the cosmic microwave background radiation (Fixsen et al. 1996). The inclusion of the cosmic microwave background has little effect on T_d at $z \lesssim 7$ in our models.

We have ignored other sources of radiation (primarily active galactic nuclei) in the heating of interstellar dust. The blue emissivity of quasars, estimated from the observed luminosity function (Pei 1995), is less than a few percent of the blue emissivity of galaxies at all redshifts in our models. The far-infrared emissivity of quasars, however, is not yet known. At long wavelengths ($h\nu \ll kT_d$), the multi-temperature spectrum $\langle B_\nu \rangle(T_d)$ reduces to the Rayleigh-Jeans part of a single blackbody with the same T_d . At short wavelengths ($h\nu \gg kT_d$), the mean spectrum exceeds the Wien tail of a single blackbody at the mean temperature.

2.3.5. Inputs from Galaxy Surveys

The formulae developed above allow us to input the observed emissivity $E_{\nu o}$ from optical imaging and redshift surveys into our models of cosmic chemical evolution. The observable $E_{\nu o}$ specifies the comoving rate of star formation $\dot{\Omega}_s$ through the relation

$$\dot{\Omega}_s(z) = \frac{1}{1 - A_\nu(z)} \left[\frac{E_{\nu o}(z)}{C_\nu(z)} \right], \quad (43)$$

where C_ν converts between the intrinsic stellar emissivity and star formation rate and A_ν corrects for the stellar photons absorbed by dust in the interstellar medium (eq. 24). Because A_ν is coupled to $\dot{\Omega}_d$ (eqs. 34 and 37) and C_ν is coupled to $\dot{\Omega}_s$ (eq. 25), solutions to our models of cosmic chemical evolution must be derived iteratively (see § 3). In the following, we adopt the observed ultraviolet emissivity $E_{\nu o}(z)$ from optical surveys of galaxies and estimate the dust temperature index α from observations of IRAS galaxies in the local universe. This then leaves two unknown parameters in our models: τ_{cV} mainly affects the overall amplitude of the absorption by dust and hence the amplitude of the far-infrared background intensity, whereas ϵ mainly affects the evolution of the dust opacity and hence the spectral shape of the background intensity. Thus, τ_{cV} and ϵ can be constrained by measurements of the cosmic far-infrared background.

Estimates of the observed ultraviolet emissivity $E_{\nu o}(z)$ are now available over the redshift interval $0.2 \lesssim z \lesssim 4.5$, from the Canada-France Redshift Survey (CFRS, Lilly et al. 1995) and the Hubble Deep Field (HDF, Williams et al. 1996). Table 2 lists the estimates of $E_{\nu o}(z)$ at several redshifts for an assumed cosmology with $\Lambda = 0$, $q_0 = 1/2$, and $H_0 = 50 \text{ km s}^{-1} \text{ Mpc}^{-1}$. The entries at $z = 0.35 - 0.875$ were derived by Lilly et al. (1996) from the rest-frame 2800 Å luminosities of about 600 galaxies in the CFRS sample with spectroscopically confirmed redshifts over $0 < z < 1$. The entries at $z = 1.25 - 1.75$ were derived by Connolly et al. (1997) from the rest-frame 2800 Å luminosities of some 200 galaxies selected

in the HDF images with photometrically estimated redshifts over $1 < z < 2$. The two entries at $z = 2.75$ and $z = 4.0$ were derived by Madau et al. (1996, 1998): the former is based on 69 ultraviolet-dropout galaxies in the HDF images with color-estimated redshifts of $2.0 \lesssim z \lesssim 3.5$, and the latter is based on 14 blue dropout galaxies with color-estimated redshifts of $3.5 \lesssim z \lesssim 4.5$. The ultraviolet emissivity at $z = 0$ is not directly observed. Instead, we use the mean B -band luminosity density of local galaxies from Ellis et al. (1996), listed as the first entry of $E_{\nu o}(z)$ in Table 2. The values of $E_{\nu o}$ derived by these authors all include modest extrapolations beyond the observed range of luminosities using a Schechter function with $\alpha \approx -1.3$. The quoted statistical uncertainties in $E_{\nu o}$ are 20 – 30% at $z \lesssim 1$ and 40 – 60% at $z \gtrsim 1$.

We determine the temperature index α of the dust by fits to the observed infrared emissivity of the local universe from the IRAS survey. The results are shown in Figure 6, where $E_{d\nu}(0)$ is normalized at $\lambda_1 = 100 \mu\text{m}$, so that the ratio of $E_{d\nu}(0)/E_{d\nu_1}(0)$ depends mainly on α . The data points were derived by Soifer & Neugebauer (1991) from complete flux-limited samples ($z \leq 0.08$ and $\langle z \rangle = 0.006$) at $\lambda = 12, 25, 60$, and $100 \mu\text{m}$. The plotted errors reflect statistical uncertainties in the corresponding luminosity functions tabulated by Soifer

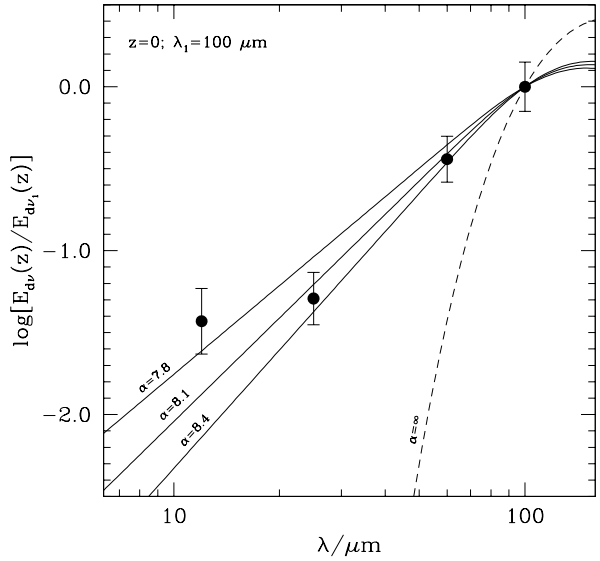


FIG. 6.—Normalized infrared emissivity at $z = 0$. The data points were derived by Soifer & Neugebauer (1991) from IRAS observations of nearby galaxies at $\lambda = 12, 25, 60$, and $100 \mu\text{m}$. The solid curves represent the multi-temperature models of dust emission with the indicated values of the temperature index α , while the dashed curve represents a single blackbody.

& Neugebauer (1991). The solid curves show the multi-temperature models with the three indicated values of α , while the dashed curve shows a single blackbody (with $\alpha = \infty$). All curves are computed with $\kappa_a \propto \nu^2$, an approximation at $\lambda \gtrsim 10 \mu\text{m}$ for LMC-type dust (§ 2.2.5), and $T_d(0) = 16.5 \text{ K}$, a typical mean temperature of dust at $z = 0$ obtained in our models (§ 3.3), but these curves are insensitive to the exact value of T_d , varying by roughly 30% at $12 \mu\text{m}$ for $T_d \approx 10 - 25 \text{ K}$. In the context of this work, namely, using the cosmic infrared background to correct for any missing starlight in the optical data, it is important to have a good account of the total infrared energy of the dust emission. A single blackbody, if adopted, would underestimate the mid-infrared emission, missing roughly 50% of the total infrared energy. We adopt the multi-temperature spectrum with $\alpha = 8.1$ in all of our calculations. This still underestimates the emission near $12 \mu\text{m}$. The observed excess is believed to be contributed by very small grains (including polycyclic aromatic hydrocarbons), which can be excited by single photon hits and produce non-thermal emission with complex emission features (Désert et al. 1990). Never-

theless, the mid-infrared excess near $12 \mu\text{m}$ contributes less than 10% of the total infrared energy and hence should have little effect on our fits to the cosmic infrared background.

3. RESULTS

Our models of cosmic chemical evolution are specified by equations (4)-(6). These equations link the history of metal enrichment to the histories of star formation and gas consumption in galaxies and the baryon flow between the interstellar and intergalactic media. We adopt two observational inputs to solve the models: (1) the observed comoving density of HI, Ω_{HIo} , from damped Ly α surveys, and (2) the observed ultraviolet emissivity of galaxies, $E_{\nu o}$, from optical imaging and redshift surveys. The first is related to the comoving density of gas, Ω_g , (eq. 19), including a correction factor, Q , for the absorbers missing from existing damped Ly α surveys that is self-consistently coupled to the comoving density of dust (eq. 17). The second is related to the comoving rate of star formation, $\dot{\Omega}_s$, (eq. 43), which depends on

TABLE 1
MODEL INPUTS

Parameter	Value	Source
Present mean metallicity	$Z(0) = Z_{\odot} = 0.02$	solar value
Mean dust-to-metals ratio	$d_m = 0.45 \pm 0.1$	fit - Fig. 1
Slope of bright quasar counts	$\beta = 2.0 \pm 0.1$	fit - Fig. 2
Index of gamma distribution	$\gamma = 1.2 \pm 0.1$	fit - Fig. 3
Norm of gamma distribution	$f_* = 0.03 \pm 0.01$	fit - Fig. 3
Index of temperature distribution	$\alpha = 8.1 \pm 0.3$	fit - Fig. 6
Opacities of grains κ_e & κ_a	LMC-type dust	model - Fig. 4
Population synthesis F_{ν} & R	Salpeter IMF, $0.1 - 100 M_{\odot}$	model - Fig. 5
Observed density of HI $\Omega_{\text{HIo}}(z)$	Data - absorption surveys	listed in Tab. 2
Observed UV emissivity $E_{\nu o}(z)$	Data - optical surveys	listed in Tab. 2
Small-scale clumpy ISM model	$(\tau_{cV}, \epsilon) = \begin{cases} (1.13, 1.0) \\ (1.06, 0.4) \\ (1.13, 0.1) \end{cases}$	minimum J_{ν} fit
		best J_{ν} fit
		maximum J_{ν} fit

NOTE.—The present mean metallicity $Z(0)$ is taken to be the solar value (§ 2.1). The dust-to-metals mass ratio d_m is the mean value in nearby galaxies and damped Ly α systems at $0.7 \leq z \leq 2.8$ (§ 2.1). The bright-end slope β of the luminosity function of quasars is fitted from the observed counts at $B \leq 20$ (§ 2.2.3). The gamma distribution parameters γ and f_* for the distribution of HI column densities are fitted from surveys of damped Ly α systems (§ 2.2.3). The dust temperature index α is estimated from the mean infrared colors of local galaxies (§ 2.3.5). The extinction and absorption opacities of dust grains, κ_e and κ_a , are derived from the graphite-silicates model that fits the observed LMC extinction curve (§ 2.2.5). The population synthesis spectrum F_{ν} and returned fraction R are computed from the latest version of the Bruzual-Charlot models with a Salpeter IMF truncated at 0.1 and $100 M_{\odot}$ (§ 2.3.2). The present visual optical depth τ_{cV} of small-scale dust clumps and the evolution index ϵ of the clumps relative to the global chemical enrichment history of galaxies are determined from fits to the DIRBE and FIRAS measurements of the cosmic infrared background (§ 3.4).

a conversion factor, C_ν , between the intrinsic emissivity and star formation rate (with the aid of stellar population synthesis models in eq. 25) and a correction factor, A_ν , for stellar radiation absorbed by dust within galaxies that is again self-consistently coupled to the comoving density of dust (eq. 37). The background intensity, J_ν , at the present epoch is given by equation (21), including the radiation from both stars (eq. 24) and dust (eq. 39).

Table 1 lists all the input parameters of our models. The only adjustable parameters are the present visual optical depth τ_{cV} of small-scale clumps of dust and the index ϵ that specifies the evolution of these clumps relative to the mean comoving density of dust (§ 2.3.3). Since the obscuration, absorption, and emission by dust are interrelated, all the equations in our models are coupled. Iterative solutions are obtained as follows. Given τ_{cV} and ϵ , the initial set of Ω_g and $\dot{\Omega}_s$ (and hence all other quantities as functions of redshift in our models) is computed with $Q = 1$, $A_\nu = 0$, and C_ν from a constant $\dot{\Omega}_s$. The values of Q , A_ν , and C_ν are then updated from this initial solution so that the next solution can be computed. This iterative process is repeated until Ω_g and $\dot{\Omega}_s$ (and hence all the other quantities) converge at all redshifts. The stellar and dust emissivities, $E_{s\nu}$

and $E_{d\nu}$, as functions of z , and the background intensity, J_ν , at $z = 0$ are then computed from the converged solutions. Fits of the far-infrared part of J_ν to the background measurements then give the values of τ_{cV} and ϵ . These parameters are not strongly correlated; τ_{cV} determines mostly the amplitude of the far-infrared background, while ϵ controls mostly the spectral shape of the background. In addition to the best-fit solution, we also present the 95% confidence minimum and maximum solutions to bracket the observational uncertainties in the infrared background measurements (described in detail in § 3.4). The corresponding values of τ_{cV} and ϵ are listed in Table 1.

3.1. Interstellar Gas and Star Formation

The comoving density of interstellar gas Ω_g and the comoving rate of star formation $\dot{\Omega}_s$ are the two key quantities from which all other quantities in our models can be calculated. Table 2 lists selected solutions (Ω_g , Z , $\dot{\Omega}_s$, A_ν), together with the input data Ω_{HIIo} and $E_{\nu o}$. We have adopted discrete input data, because $\Omega_{\text{HIIo}}(z)$ at different z is obtained from samples of quasars selected at different effective wavelengths λ_e , while $E_{\nu o}(z)$ at dif-

TABLE 2
SELECTED SOLUTIONS

z	$\Omega_{\text{HIIo}}(z)$	λ_e	$\Omega_g(z)$	$Z(z)/Z_\odot$
0.00	(0.25)	5500	0.50 ± 0.12	(1.000)
0.64	0.54 ± 0.31	5500	2.28 (1.90, 2.45)	0.511 (0.473, 0.524)
1.89	1.58 ± 0.92	5500	6.58 (4.04, 8.43)	0.102 (0.076, 0.111)
2.40	2.15 ± 0.70	5500	6.88 (4.23, 9.68)	0.060 (0.036, 0.070)
3.17	2.34 ± 1.14	5500	4.66 (3.65, 6.65)	0.026 (0.013, 0.040)
4.01	1.44 ± 0.58	6500	2.15 (1.99, 2.63)	0.016 (0.008, 0.035)
z	$\log E_{\nu o}(z)$	λ	$\dot{\Omega}_s(z)$	$A_\nu(z)$
0.000	19.47 ± 0.10	4400	0.60 (0.66, 0.63)	0.468 (0.486, 0.487)
0.350	18.89 ± 0.07	2800	1.97 (2.63, 1.86)	0.645 (0.718, 0.627)
0.625	19.21 ± 0.08	2800	4.88 (6.52, 4.23)	0.688 (0.758, 0.650)
0.875	19.53 ± 0.15	2800	11.2 (15.0, 9.66)	0.691 (0.760, 0.651)
1.250	19.69 ± 0.15	2800	17.0 (19.9, 15.3)	0.671 (0.704, 0.642)
1.750	19.59 ± 0.15	2800	11.1 (9.13, 10.6)	0.630 (0.507, 0.635)
2.750	19.42 ± 0.15	1500	14.7 (4.72, 20.5)	0.823 (0.472, 0.874)
4.000	19.02 ± 0.20	1500	2.97 (1.21, 7.29)	0.637 (0.118, 0.848)

NOTE.—Input quantities are listed in the form observation $\pm 1\sigma$ uncertainty. Output quantities are listed in the form best (minimum, maximum) solutions allowed by the cosmic far-infrared background. All entries pertain to $\Lambda = 0$, $q_0 = 1/2$, and $H_0 = 50 \text{ km s}^{-1} \text{ Mpc}^{-1}$; Ω_{HIIo} and Ω_g in units of 10^{-3} , λ_e and λ in units of \AA , $E_{\nu o}$ in units of $\text{W Hz}^{-1} \text{ Mpc}^{-3}$, $\dot{\Omega}_s$ in units of 10^{-4} Gyr^{-1} . The relation between the total and net star formation rates is $\dot{\Omega}_*(z) = (1 - R)^{-1}\dot{\Omega}_s(z)$, with $R = 0.33, 0.32, 0.31, 0.30$, and 0.28 at $z = 0, 1, 2, 3$, and 4 , respectively.

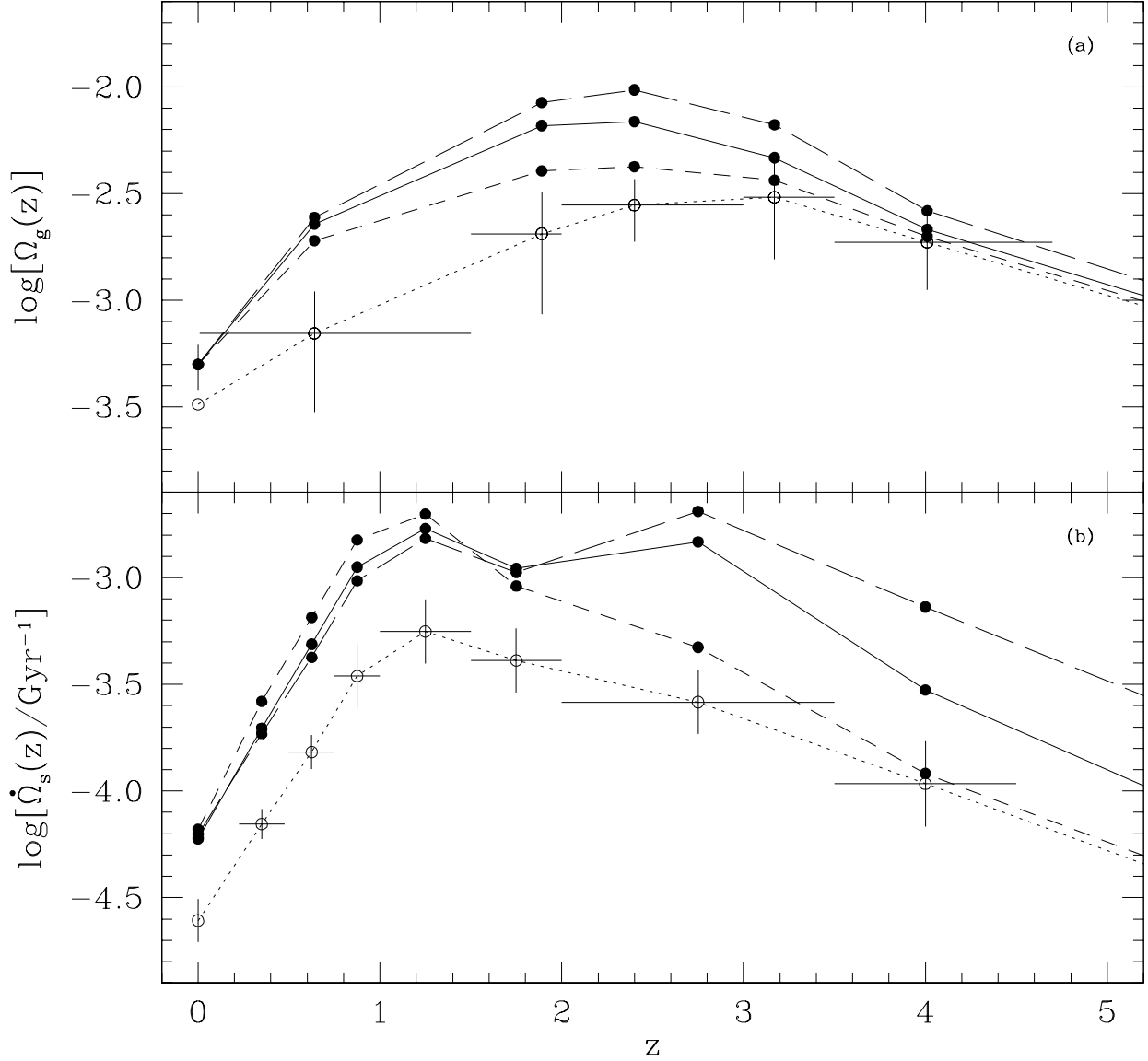


FIG. 7.—Comoving density of interstellar gas (upper panel) and comoving rate of star formation (lower panel). The filled circles are the pointwise solutions, connected by the solid, short-dash, and long-dash curves to distinguish the best, minimum, and maximum solutions, respectively. In the upper panel, the open circles with error bars, connected by the dotted curve, are the observed comoving density of neutral gas in damped Ly α systems. In the lower panel, the open circles with error bars, connected by the dotted curve, are the observed ultraviolet emissivities when expressed as star formation rates (without correction for absorption by dust).

ferent z is measured at different rest-frame wavelengths λ . Accordingly, $Q(z)$ is evaluated at the same redshifts as $\Omega_{\text{H I o}}(z)$, while $A_\nu(z)$ and $C_\nu(z)$ (averaged through a $\pm 10\%$ wavelength box filter) are evaluated at the same redshifts as $E_{\nu o}(z)$. The discrete values of $Q(z)$, $A_\nu(z)$, and $C_\nu(z)$, along with $\Omega_{\text{H I o}}(z)$ and $E_{\nu o}(z)$, are then sufficient to define the pointwise solutions for $\Omega_g(z)$ and

$\dot{\Omega}_s(z)$. To derive other functions of redshift, we interpolate in $\Omega_g(z)$ and $\dot{\Omega}_s(z)$ using the form $\log \Omega(z) \propto z$. With other interpolation schemes, such as $\log \Omega(z) \propto \log(1+z)$, the results would differ typically by a few percent, reaching only 10% at $z \approx 4$.

Figure 7 shows the comoving density of interstellar gas and the comoving rate of star formation as functions

of redshift. The filled circles are the model solutions for $\Omega_g(z)$ and $\dot{\Omega}_s(z)$, connected by the solid, short-dash, and long-dash curves to distinguish the best, minimum, and maximum (95% confidence) solutions, respectively. In the upper panel, the open circles with error bars are the observed comoving density of neutral gas in damped Ly α systems, $\mu\Omega_{\text{H I O}}$. The obscuration correction to Ω_g (from the open to filled circles) is $Q = 1.5, 2.5 - 3.7$, and $1.3 - 2.5$ at $z = 0, 1$, and 3 , where the ranges include the three solutions. This correction is large at $z \approx 1$, when the comoving density of dust is near its highest value. The peak in Ω_g occurs at $z \approx 2.4$, just before gas is consumed faster by star formation than it is replenished by inflow. In the lower panel, the open circles with error bars are the observed (i.e., optically inferred) star formation rates derived in the absence of dust absorption, $E_{\nu o}/C_\nu$. The absorption correction to $\dot{\Omega}_s$ (from the open to filled circles) is $(1 - A_\nu)^{-1} = 2.4 - 2.5, 2.8 - 3.9$, and $1.7 - 7.8$ at $z = 0, 1$, and 3 . All three solutions for $\dot{\Omega}_s(z)$ show a rapid decrease with respect to time at $z \lesssim 1$ and an increase with time at $z \gtrsim 3$. The best and maximum solutions remain roughly flat over $1 \lesssim z \lesssim 3$, while the minimum solution still shows an increase with time over this redshift range.

The star formation rates in our models differ among the three solutions by less than 30% at $z \lesssim 2$ but by a factor of three at $z \gtrsim 3$. The similarity at low redshifts is a consequence of the constraint imposed by the far-infrared background. In our models, the mean comoving density of dust is small at high redshifts, and hence substantial absorption occurs only if the dust is extremely clumpy, as would be the case for heavily embedded stars. Indeed, we find that the minimum solution corresponds to an instantaneous mixing of dust in the interstellar medium (i.e., small-scale clumps follow the evolution of the whole interstellar medium), whereas the maximum solution corresponds roughly to an incomplete mixing of dust (i.e., small-scale clumps are nearly independent of the evolution of the rest of the interstellar medium), with the best solution representing an intermediate case. Therefore, the different solutions derived here reflect different evolution of the small-scale inhomogeneity of dust in galaxies.

3.2. Chemical Enrichment of the Interstellar Medium

Figure 8 shows the mean abundance, Z , and comoving density, Ω_m , of heavy elements in the interstellar medium as functions of redshift in our models. Again, the solid, short-dash, and long-dash curves represent the best, minimum, and maximum solutions, respectively. The data points at $z \geq 1.5$ were derived by Pettini et al. (1997b) from the observed abundances of Zn in

damped Ly α systems, while the data point at $z = 0.77$ was derived by Boissé et al. (1998) by combining their own observations with those of Pettini et al. (1997b). These are the HI column density weighted mean metallicity and hence are the correct measure of metallicity to be compared with our models. The uncertainty in the data is still large and no attempt is made here to correct for a preferential selection of the low-metallicity absorbers that would bias the observed mean. We emphasize, however, that this bias could potentially be large at $z \approx 1$, where the comoving density of dust is high. Nevertheless, all three solutions for the mean metallicity in our models are consistent within the uncertainties with the observations, especially if the data point at $z = 0.77$ is regarded as a lower limit. The present mean metallicity $Z(0)$, taken here to be the solar value, implies an effective yield of $y = 0.45Z_\odot$, nearly the same in the three solutions. The peak in Ω_m at $z \approx 0.8$ is due to a combination of the rise in Z and the decline in Ω_g toward $z = 0$. The decrease in Ω_m toward $z = 0$ is caused partly by the fact that star formation starts to consume more metals than it contributes to the interstellar medium (at $z \lesssim 0.8$, when Z exceeds y), and partly by some outflow of the interstellar metals to the intergalactic medium (see § 4.4).

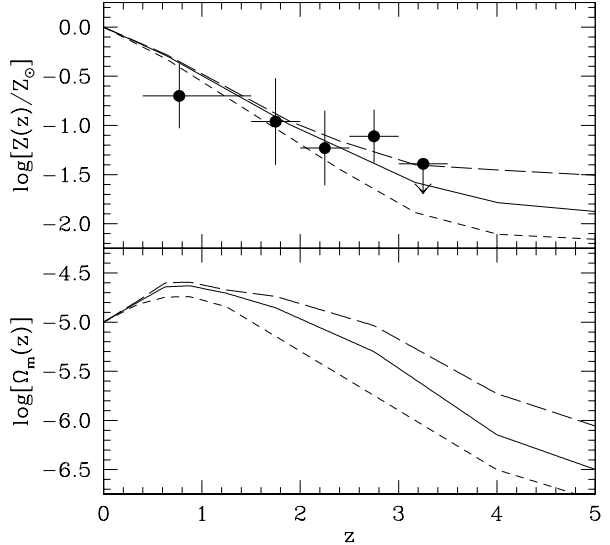


FIG. 8.—Mean metallicity of interstellar gas in galaxies in units of the solar value (upper panel) and comoving density of heavy elements in galaxies (lower panel). The solid, short-dash, and long-dash curves are the best, minimum, and maximum solutions in our models. In the upper panel, the data points at $z \geq 1.5$ are from Pettini et al. (1997b), while the data point at $z = 0.77$ is from Boissé et al. (1998).

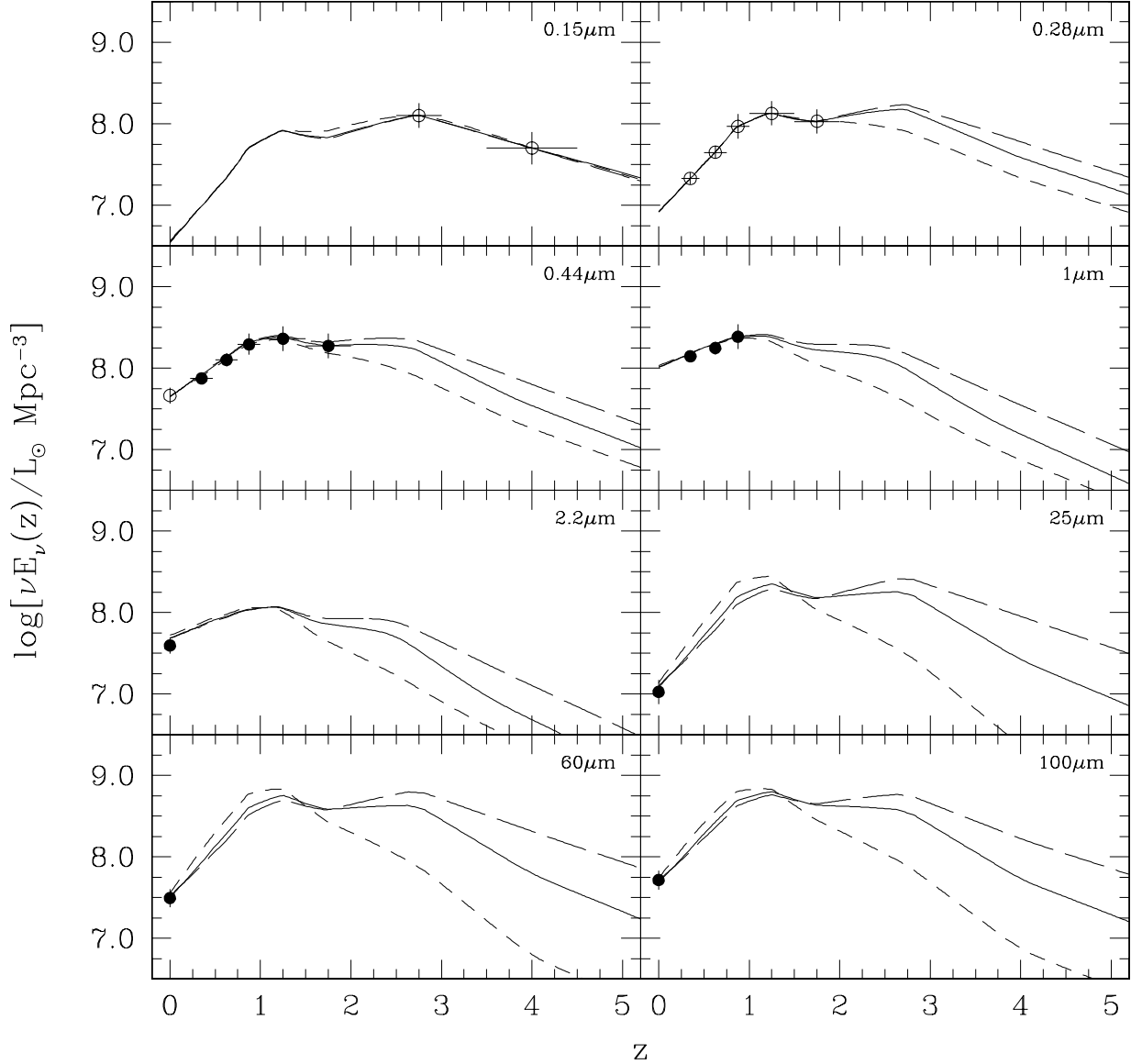


FIG. 9.—Comoving emissivity $E_\nu(z)$ times frequency ν as a function of redshift. The solid, short-dash, and long-dash curves are the best, minimum, and maximum solutions in our models. The data points are from Madau et al. (1998) for $0.15 \mu\text{m}$; Lilly et al. (1996) for 0.28 , 0.44 , and $1.0 \mu\text{m}$ at $z = 0.25 - 1.0$; Connolly et al. (1997) for 0.28 and $0.44 \mu\text{m}$ at $z = 1 - 2$; Ellis et al. (1996) for $0.44 \mu\text{m}$; Gardner et al. (1997) for $2.2 \mu\text{m}$; and Soifer & Neugebauer (1991) for 25 , 60 , and $100 \mu\text{m}$. All wavelengths are in the rest frame at the indicated redshifts.

The histories of metal enrichment in the three solutions presented here differ mainly at high redshifts and are caused by the different histories of star formation. This indicates that the observed mean metallicity in the high-redshift damped $\text{Ly}\alpha$ systems should be a useful constraint on star formation at high redshifts. In particular, if the global rates of star formation were much higher at $z \gtrsim 3$ than in the maximum solution presented

here, the interstellar metallicity would be larger than that observed in the damped $\text{Ly}\alpha$ systems, unless a significant outflow had occurred before $z \approx 3$.

3.3. Evolution of Stellar and Dust Emissivities

Figure 9 shows the emissivity $E_\nu(z)$ times frequency ν as a function of redshift at several rest-frame wave-

lengths. The data are taken from Lilly et al. (1996) for 0.28, 0.44, and 1.0 μm at $z = 0.35$, 0.625, and 0.875, Madau et al. (1998) for 0.15 μm at $z = 2.75$ and 4.0, Connolly et al. (1997) for 0.28 and 0.44 μm at $z = 1.25$ and 1.75, Ellis et al. (1996) for 0.44 μm at $z = 0$, Gardner et al. (1997) for 2.2 μm at $z = 0$, and Soifer & Neugebauer (1991) for 25, 60, and 100 μm at $z = 0$. The curves are the three solutions for the cosmic emissivity in our models. The results at $\lambda = 0.15 - 2.2 \mu\text{m}$ represent the direct but attenuated starlight, while those at $\lambda = 25 - 100 \mu\text{m}$ represent the starlight reradiated by dust. The data that were input to the models are plotted as open circles, while those that are output are plotted as filled circles. Evidently, our models reproduce remarkably well even data that were not used as input. In particular, the agreement at $\lambda = 1.0 - 2.2 \mu\text{m}$, where the absorption by dust is relatively small, is an indication that the Salpeter IMF is reasonable. A steeper IMF, such as a Scalo IMF, would produce too much 2.2 μm light at $z = 0$ (by a factor of two). The agreement with the observed 25 – 100 μm emissivity at $z = 0$ indicates that the evolution of the small-scale clumpiness of dust in the models is reasonable. A substantially different evolution from that presented here might give an acceptable fit to the integrated infrared background but would not necessarily match the local infrared emissivity at the same time.

The mean temperature of dust, plotted in the upper

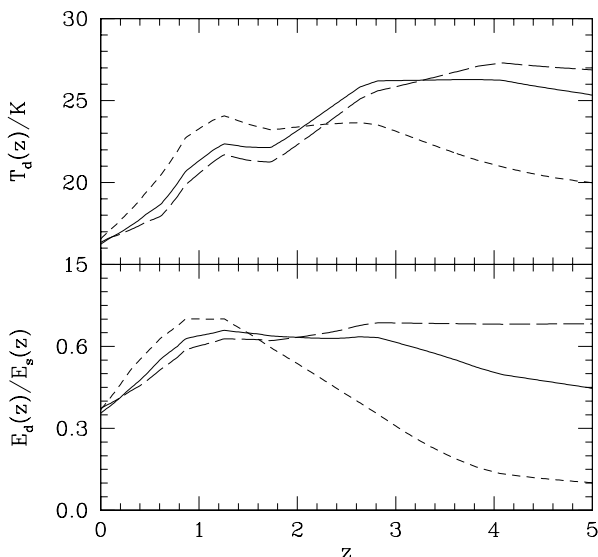


FIG. 10.—Mean temperature of interstellar dust (upper panel) and ratio of bolometric dust emissivity to bolometric stellar emissivity (lower panel). The solid, short-dash, and long-dash curves represent the best, minimum, and maximum solutions, respectively.

panel of Figure 10, varies from $T_d = 21 - 27 \text{ K}$ at $z = 4$ to $T_d = 22 - 24 \text{ K}$ at $z = 2$ and then decreases to $T_d = 16.5 \text{ K}$ at $z = 0$. In our models, dust grains heated to different temperatures (at least above a finite temperature $T_c \approx 0.9T_d$) contribute different amounts to the bolometric dust emission: 50% by dust with $T \approx (0.9 - 1.6)T_d$, 25% by dust with $T \approx (1.6 - 3.0)T_d$, and 25% by dust with $T \gtrsim 3.0T_d$, with little dependence on redshift. The ratio of the bolometric dust emission to the bolometric stellar emission, defined by $E_d/E_s = \int d\nu E_{d\nu} / \int d\nu E_{s\nu}$ and plotted in the lower panel of Figure 10, varies from $E_d/E_s = 14 - 68\%$ at $z = 4$ to $E_d/E_s = 54 - 64\%$ at $z = 2$ and then decreases to $E_d/E_s = 36\%$ at $z = 0$. Evidently, the dust absorbs and reradiates a significant fraction of the stellar energy. Moreover, since τ_c is typically larger than τ_t , most of this absorption occurs in small-scale clumps, rather than the large-scale distribution of dust in the interstellar medium. This is consistent with the general notion that the young stars responsible for most of the energy production are typically located in dusty star-forming regions.

3.4. Cosmic Background Radiation

Figure 11 shows the background intensity J_ν at $z = 0$ times frequency ν as a function of wavelength λ . The circles at 140 and 240 μm are the DIRBE detections; the errors include both statistical and systematic uncertainties in the measurements and the removal of foreground emissions (Hauser et al. 1998). The zigzag curve at 150 – 2000 μm is the weighted mean of the FIRAS detections, based on three independent methods to remove the foregrounds (Fixsen et al. 1998). The statistical uncertainties in the FIRAS results are 40%, 27%, 5%, 6%, 10%, and 15% at $\lambda = 160, 180, 240, 400, 700$, and 1000 μm , respectively (Fixsen 1998, private communication). The solid curve is the weighted minimum- χ^2 fit of the background intensity in our models to the far-infrared/submillimeter DIRBE and FIRAS measurements to determine τ_{cV} and ϵ . We regard this as our “best” solution. The systematic uncertainties in the FIRAS results are not known precisely. For this reason, two other acceptable fits are presented as the short-dash and long-dash curves. These “minimum” and “maximum” solutions would be the 95% confidence lower and upper limits if the systematic uncertainties in the FIRAS data were taken to be the difference between the three independent methods in the removal of the foregrounds by Fixsen et al. (1998).

Also shown in Figure 11 is a comparison of the backgrounds in our models with various measurements and limits at other wavelengths. The squares with errors

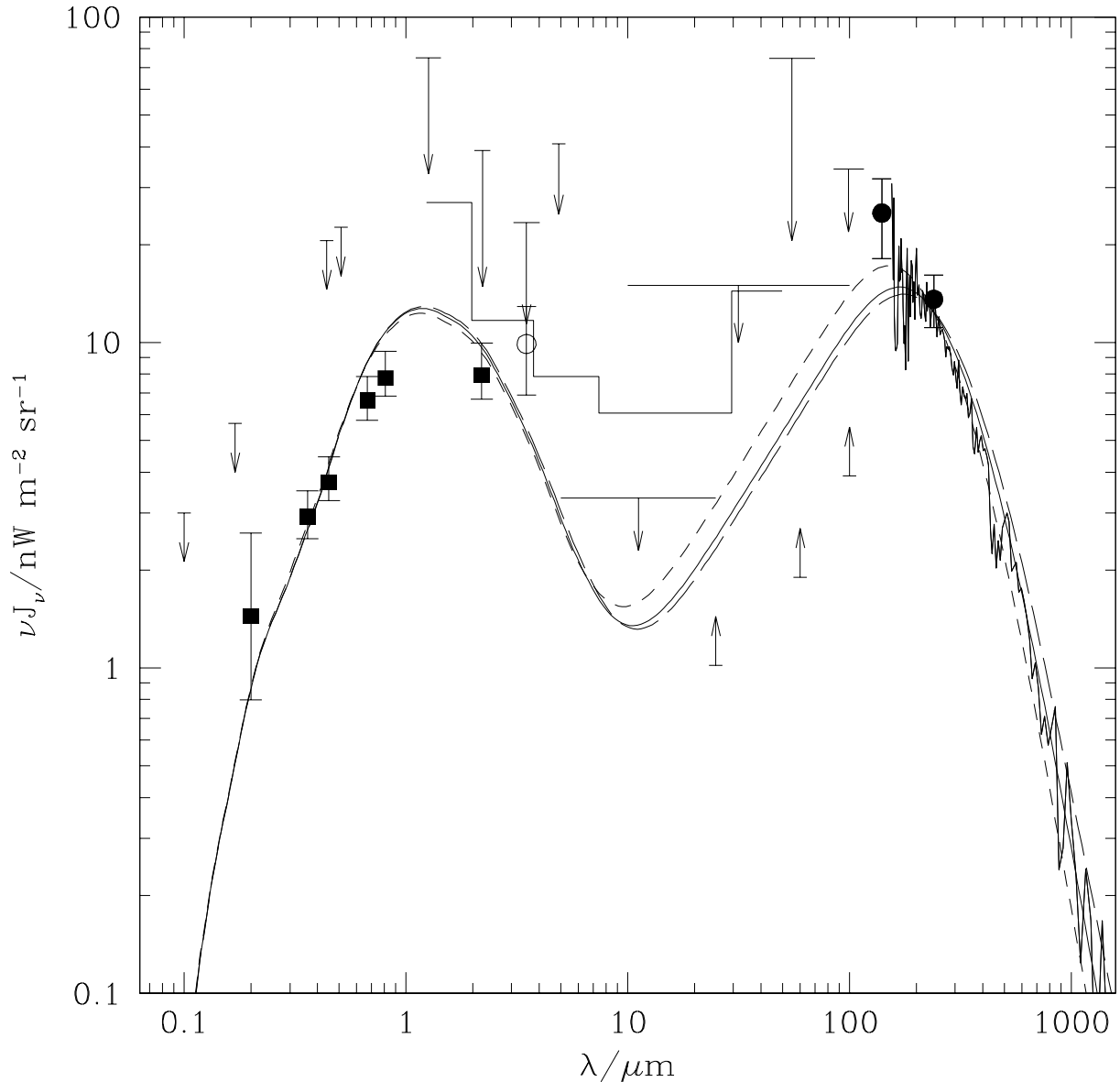


FIG. 11.—Extragalactic background intensity J_ν times frequency ν as a function of wavelength λ . The circles are the DIRBE detections of the cosmic infrared background at 140 and 240 μm (Hauser et al. 1998). The zigzag curve is the FIRAS detections at 150 – 2000 μm (Fixsen et al. 1998). The solid, short-dash, and long-dash curves represent the best, minimum, and maximum fits of our models to these observations. The filled squares are the integrated background light from galaxy counts at 2000 \AA (Armand et al. 1994) and 3600 – 22000 \AA (Pozzetti et al. 1998). The open circle is a tentative detection of the extragalactic background at 3.5 μm (Dwek & Arendt 1998). The arrows and the stepped line indicate various observational limits on the extragalactic background radiation (see § 3.4 for references).

are the integrated light from observed sources at 2000 \AA (Armand, Milliard, Deharveng 1994) and 3600 – 22000 \AA (Pozzetti et al. 1998). The large error at 2000 \AA is due to the extrapolation of the counts beyond a limiting magnitude of 18.5. At optical wavelengths, the slope of the

counts suggests that very faint uncounted galaxies contribute little to the background. Thus, we regard the integrated light from the observed sources as tantamount to a measurement of rather than a lower limit on the background. The open circle is a tentative detection of

the extragalactic background at $\lambda = 3.5 \mu\text{m}$ from the DIRBE (2.2 and $3.5 \mu\text{m}$) maps and an assumed value of the background at $\lambda = 2.2 \mu\text{m}$ by Dwek & Arendt (1998). Various (downward and upward) arrows are observational (upper and lower) limits: the DIRBE 2σ upper limits at $1.25 - 100 \mu\text{m}$ (Hauser et al. 1998), the high galactic latitude upper limits at 1000 \AA (Holberg 1986) and 1700 \AA (Bowyer 1991), the sky surface photometry upper limits at 4400 \AA (Toller 1983) and 5100 \AA (Dube, Wickes, & Wilkinson 1979), the lower limits in the no-evolution case from IRAS galaxy counts at 25, 60, and $100 \mu\text{m}$ (Hacking & Soifer 1991), the upper limits at $10 - 100 \mu\text{m}$ from the fluctuation analysis of the DIRBE maps (Kashlinsky, Mather, & Odenwald 1996), and the upper limits at $5 - 25 \mu\text{m}$ (Stanev & Franceschini 1998) and at $1 - 50 \mu\text{m}$ (stepped line, Biller et al. 1998) from the lack of attenuation in the TeV gamma-ray spectrum of Mrk 501. Evidently, our models agree well with a wide variety of measurements of and limits on the background intensity over four decades in wavelengths.

The total energy density radiated by stars of all ages and now contained in the extragalactic background (over $912 \text{ \AA} \leq \lambda \leq 5 \text{ mm}$) is, in units of the present critical energy density,

$$\Omega_R \equiv \frac{32\pi^2 G}{3H_0^2 c^3} \int_0^\infty d\nu J_\nu = (5.1 - 5.5) \times 10^{-6}. \quad (44)$$

Of this, 54–59% is reprocessed by dust into the cosmic infrared background. For comparison, the energy density in the cosmic microwave background radiation left by the Big Bang is about 20 times larger than that given by equation (44) (Fixsen et al. 1996). In these estimates, we have ignored the unknown contribution from active galactic nuclei.

4. DISCUSSION

We have combined our models with a wide variety of observations to study the average evolution of the entire population of galaxies. Before discussing some implications of our solutions (§ 4.4 and § 4.5), we examine some major uncertainties that could potentially affect our results (§ 4.1 and § 4.2) and compare them with other estimates (§ 4.3).

All of the results presented here are based on a cosmological model with $\Lambda = 0$, $q_0 = 1/2$, and $H_0 = 50 \text{ km s}^{-1} \text{ Mpc}^{-1}$. These parameters may no longer be regarded as “standard” in light of recent evidence, especially from high-redshift supernovae (see, for example, Reiss et al. 1998). However, many of the observational input data on which our results depend were reported only for this particular set of cosmological parameters. A self-consistent exploration of the effects of different

cosmological parameters would therefore require a re-analysis of the input data, particularly $\Omega_{\text{HI}o}$ and $E_{\nu o}$. Such a study might prove interesting but is beyond the scope of this paper.

4.1. Model Uncertainties

Our results are independent of many properties of the damped Ly α systems, including their morphologies, provided only that they represent the main reservoirs of gas for star formation. The existing evidence, although not yet conclusive, suggests that the damped Ly α systems are galaxies of a wide variety of morphological types (Le Brun et al. 1997). The idea that the damped Ly α systems trace the bulk of star formation is supported by the observation that they contain enough neutral gas at $z \approx 2 - 3$ to make all the stars visible today (Wolfe et al. 1995). Such a large amount of neutral gas is not present in the local universe, even including the contribution of low surface brightness and dwarf galaxies (Zwaan et al. 1997). Indeed, if the neutral gas in damped Ly α systems were not converted into stars, it must have been expelled or ionized at low redshifts.

The main approximation in our treatment of the interstellar gas in galaxies is the neglect of molecules. As discussed in § 2.2.1, this could increase Ω_g by up to a factor of two, most likely at low redshifts. Accordingly, Ω_d would be also be higher because it is linked to the metallicity and the present value $Z(0)$ is fixed in our approach. However, as we have already emphasized, $Z(0)$ is not known precisely, and different values of this parameter affect Ω_d through Ω_g as well. We have checked that these uncertainties, comparable to the errors in the observed comoving density of HI at low redshifts, do not strongly affect our solutions for the global rate of star formation. We have also checked that the uncertainties in the input parameters ($d_m, \beta, \gamma, f_*, \alpha$) all have minor effects on our results.

A natural consequence of dust in galaxies is that it obscures background quasars (Ostriker & Heisler 1984). This effect also causes incompleteness in samples of damped Ly α systems found in the spectra of optically selected quasars (Fall & Pei 1993). If this bias were ignored in our models, the resulting mean interstellar metallicity at $z \approx 2.5$ would be 3–5 times higher than that observed in the damped Ly α systems. As discussed at length in § 2.2.2, our models include self-consistent corrections for missing damped Ly α systems and quasars. From our solutions for f and f_o and the formulae of Fall & Pei (1993), we estimate that the missing fraction of optically selected quasars with $V \lesssim 20$ ($R \lesssim 20$) is relatively small: 9–12% (8–11%), 12–19% (10–17%), and 13–23% (12–21%) at $z = 2, 3$, and

4, respectively. An important observational constraint on obscuration comes from counts of radio and optically selected quasars on the assumption that they have the same intrinsic evolution. Shaver et al. (1996) found that the comoving densities of radio and optically selected quasars have similar apparent evolution to $z \approx 4$. However, the samples at high redshift are very small and are easily consistent with 40 – 50% of the optically selected quasars being missed at $z \approx 3-4$ (see Fig. 2 of Shaver et al. 1996). The obscuration in our models is well within this limit.

The determination of the global star formation rate from the observed ultraviolet emissivity of galaxies involves assumptions about the IMF and about dust (eq. 43). In our approach, all uncertainties in the IMF (its shape, mass cutoffs, and any redshift evolution) are combined in the conversion factor $C_\nu(z)$ between the intrinsic emissivity and star formation rate (§ 2.3.2). All uncertainties related to the dust (its opacity, evolution, and distribution) are combined in the mean fraction $A_\nu(z)$ of photons absorbed by dust (§ 2.3.3). Our solutions are based on the following assumptions: (1) an IMF that is constant in time; (2) an IMF with Salpeter form; (3) a constant dust-to-gas ratio and a power-law relation between the optical depth of small-scale clumpiness and mean comoving density of dust; (4) optical opacity of grains as in LMC-type dust; and (5) infrared opacity as in LMC-type dust. We now discuss each assumption in turn. The basic conclusion is that the small-scale clumpiness of the dust and the optical opacity of grains are the major sources of uncertainty in the determination of the global star formation history.

(1) Some of the main inputs to our models are the observed rest-frame 1500 Å and 2800 Å emissivities. These models, with a constant IMF, also reproduce as output the observed rest-frame 4400 Å and 1 μm emissivities at $0.2 \lesssim z \lesssim 2.0$ (Fig. 9). This may be an indication that any evolution of the IMF is relatively weak, at least for $z \lesssim 2$. Since absorption by dust decreases with wavelength, the rest-frame 2.2 μm emissivity of galaxies, if observed over a similar range of redshifts, could provide a tighter constraint on this evolution than the rest-frame 4400 Å and 1 μm emissivities.

(2) The Salpeter IMF is flatter (has more massive stars) than the Scalo IMF, the other IMF often employed in studies of stellar populations. The appropriateness of the Salpeter IMF over the Scalo IMF to reproduce the observed emissivities at $z = 0$ has already been noted by Lilly et al. (1996) and Madau et al. (1998). Repeating all of our calculations with a Scalo IMF, we find that the solutions for $\dot{\Omega}_s(z)$ are not strongly affected, except at very low redshifts ($z \lesssim 0.5$). However, a Scalo IMF would predict too much red light, causing a factor of

roughly 2 – 3 mismatch of our models with the observed 2.2 μm local emissivity and with the 1 – 2.2 μm extragalactic background. We have not fine-tuned the upper and lower mass cutoffs of the IMF. The lower mass cutoff could potentially affect the overall amplitude of the star formation rate, without any strong effects on the stellar emissivity. With a lower mass cutoff of $0.1 M_\odot$, the comoving density of stars at $z = 0$ in our models agrees well with the empirical estimates (§ 4.3).

(3) Our models of cosmic chemical evolution represent a self-consistent way to relate the evolution of dust to the history of star formation on the assumption of a constant dust-to-metals ratio. If this ratio were to vary by 50% over $0 \lesssim z \lesssim 3$ (Fig. 1), it would have a minor effect on the solutions for $\dot{\Omega}_s(z)$. We have adopted a simple statistical approach to characterize the small-scale clumpiness of dust in the interstellar medium. This introduces two adjustable parameters: the present value of the optical depth of the clumps τ_c and an index ϵ that specifies how the clumps evolve relative to the mean comoving density of dust. In our models, the small-scale clumpiness of dust is responsible for most of the absorption of starlight. We have presented three solutions in which the small-scale clumpiness of the dust evolve differently. This turns out to be a major source of uncertainty in our solutions for the global star formation rate.

(4) The optical opacity of grains varies between galaxies by a factor of two, even among the Milky Way, LMC, and SMC (Fig. 4). To assess this effect on our results, we repeated our calculations with Galactic and SMC-type dust. The resulting infrared background was similar within 30%, while the ultraviolet background at $\lambda \approx 2000$ Å differed by a factor of two higher (lower) for Galactic-type (SMC-type) dust relative to the LMC-type dust. The emissivity $E_{\nu o}$ at rest-frame ultraviolet wavelengths increased (decreased) by a factor of two at low redshifts and decreased (increased) at high redshifts. The solution for $\dot{\Omega}_s(z)$ was similar at $z \lesssim 2$ but a factor of two lower (higher) at $z \gtrsim 3$. These differences are consequences of the fact that Galactic-type (SMC-type) dust selectively absorbs less (more) ultraviolet radiation than the LMC-type dust. Therefore, the high- z solutions of $\dot{\Omega}_s(z)$ are uncertain (by a factor of two) due to the uncertainty in the optical opacity of grains, comparable to or less than the uncertainty caused by the small-scale clumpiness of the dust. The solutions presented here are all based on LMC-type dust, because this is an intermediate case between Galactic and SMC-type dust and because, in combination with a Salpeter IMF, it seems to account well for all the available data.

(5) The infrared opacity of grains, responsible for the dust emission, is approximated here by a power law,

$\kappa_a(\nu) \propto \nu^n$, where the normalization and index ($n = 2$) are fixed by our adopted LMC-type dust (see Fig. 4). The normalization has roughly the same effect as τ_{cV} on the amplitude of J_ν , while the index has roughly the same effect as ϵ on the shape of J_ν . Since our fits to the cosmic infrared background involve adjustment of τ_{cV} and ϵ , the uncertainties in the infrared opacity of grains are partially absorbed by these parameters. We have checked that a different infrared opacity (within 50% of the LMC-type dust) would have only minor effects on our results (but with different values of τ_{cV} and ϵ). However, if the normalization were much higher (lower) than adopted here, it would require much more (less) absorption of stellar energy to reproduce the same infrared background, causing the optical background to be too blue (red). A value of $n = 1.5$ would only give a marginally acceptable fit to the far-infrared background.

4.2. Observational Uncertainties

We have used as input to our models the best determinations available in 1997 of the comoving density of HI and the rest-frame ultraviolet emissivity, $\Omega_{\text{HI}o}$ and $E_{\nu o}$. Any errors in $\Omega_{\text{HI}o}$ and $E_{\nu o}$ would propagate into the corresponding solutions for Ω_g and $\dot{\Omega}_s$. Since the quoted statistical errors in $\Omega_{\text{HI}o}$ and $E_{\nu o}$ are all 60% or less, these uncertainties do not strongly affect our results. In addition to the statistical errors, however, it is always possible that the input data are plagued by unknown systematic errors and/or biases. After completing this work, we became aware of new estimates of $E_{\nu o}$ at high redshifts by Steidel et al. (1999) from a large ground-based survey of Lyman-break galaxies: $\log E_{\nu o} = 19.42 \pm 0.07$ at $z = 3.04$ and $\log E_{\nu o} = 19.33 \pm 0.10$ at $z = 4.13$, both for $\lambda = 1500 \text{ \AA}$ and by integrating a Schechter luminosity function down to $0.1 L_*$ (Steidel 1999, private communication). The new estimate of $E_{\nu o}$ at $z \approx 4$ is higher than the previous one by Madau et al. (1998) from the HDF by a factor of two. Steidel et al. (1999) suggest that the reason for this discrepancy is that the HDF may be too small to be a fair sample of the universe. Another source of uncertainty in $E_{\nu o}$ is the fact that the faint end of the luminosity function has not been well established at high redshifts.

We have repeated all our calculations with the new estimates of $E_{\nu o}$ by Steidel et al. (1999) at $z \geq 3$ and the entries in Table 2 at lower redshifts. We then readjusted the parameters τ_{cV} and ϵ in the models to match the cosmic far-infrared background measurements. The resulting best, minimum, and maximum solutions for $\dot{\Omega}_s$ are plotted in Figure 12, with $(\tau_{cV}, \epsilon) = (0.82, 0.8)$, $(0.98, 1.4)$, and $(0.88, 0.4)$, respectively. These solutions are not radically different from those shown in Figure

7b. The largest difference between the best solutions in the two cases is only 50% at $z \lesssim 4$, even though the corresponding input values of $E_{\nu o}$ at $z \approx 4$ differ by a factor of two. The reason for this is that our solutions for $\dot{\Omega}_s$ are constrained by many observational input data and hence the propagation of errors from $E_{\nu o}$ to $\dot{\Omega}_s$ is significantly reduced (by a factor of two at $z \approx 4$). Given these uncertainties in the input data, the global rate of star formation is fairly well determined by our models.

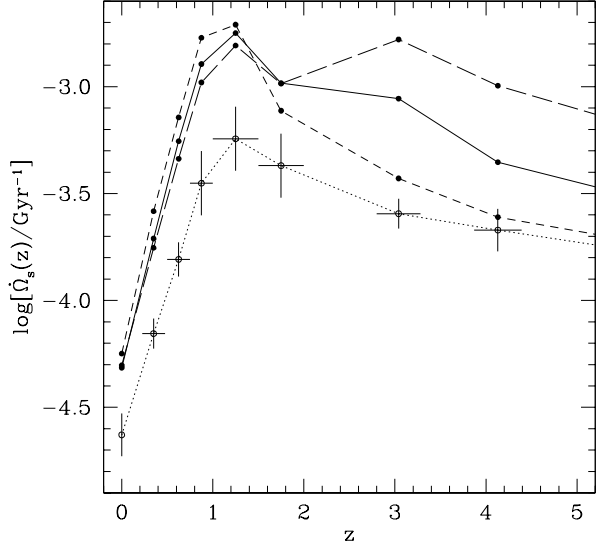


FIG. 12.—Comoving rate of star formation in our models based on the modified emissivities at $z \geq 3$ from Steidel et al. (1999). The symbols have the same meaning as in Fig. 7b.

4.3. Comparisons with Other Results

The global rates of star formation derived here are compared with independent estimates made by other techniques in Figure 13. The solid, short-dash, and long-dash curves are respectively the best, minimum, and maximum solutions for $\dot{\Omega}_s(z)$ in our models. The dotted curves are the predictions of the inflow (upper curve) and outflow (lower curve) models of Pei & Fall (1995), which are based on absorption-line observations of damped Ly α systems. The circles at $z = 0, 0.2$, and 0.8 , come from H α observations of galaxies in a local sample (Gallego et al. 1995) and in the CFRS sample (Tresse & Maddox 1998; Glazebrook et al. 1999). For consistency, we have adopted the Glazebrook et al. (1999) conversion from the H α luminosity density $L_{\text{H}\alpha}$ (corrected for dust using H β -to-H α line ratios) to the star formation rate (appropriate for the Salpeter IMF with solar metallicity), equivalent to $(\dot{\Omega}_*/\text{Gyr}^{-1}) =$

$1.0 \times 10^{-43} (L_{\text{H}\alpha} / \text{erg s}^{-1} \text{ Mpc}^{-3})$. A similar conversion factor is also found in our models (assuming 0.45 H α photons per Lyman continuum photon for case B recombination and including the metallicity dependence of the spectral evolution). The squares at $z \approx 0.2 - 1.0$ come from ultraviolet, optical, near-infrared, and radio observations of ISO 15 μm selected galaxies in the CFRS survey (Flores et al. 1999). Clearly, our solutions for the global rates of star formation agree well with the available H α and mid-infrared surveys at $z \lesssim 1$. They are also consistent with an estimate of the star formation rate at $z \approx 3$ by Hughes et al. (1998) from submillimeter observations of the HDF with SCUBA, although this depends on only a few detected sources and assumptions about their dust temperatures and redshifts (see additional results from Barger et al. 1998). The global history of star formation derived here is also broadly consistent with recent estimates of the redshift distribution of SCUBA sources (Lilly et al. 1999).

In summary, we conclude that our solutions for the

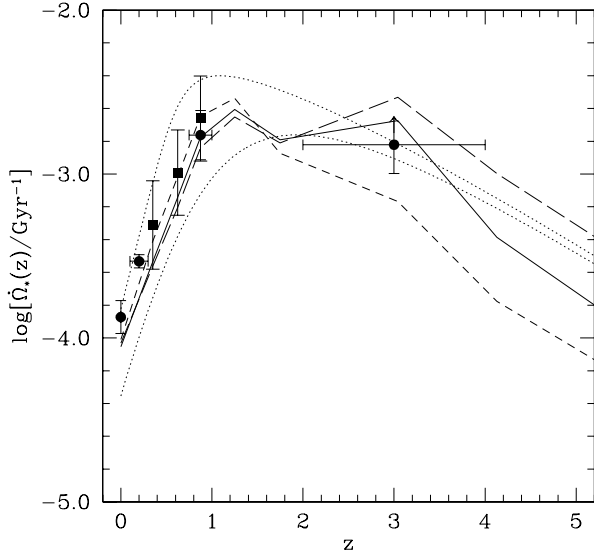


FIG. 13.—Comparisons of the comoving rate of star formation in our models with estimates from recent H α , mid-infrared, and submillimeter observations. The solid, short-dash, and long-dash curves are respectively the best, minimum, and maximum solutions derived here. The two dotted curves are the predictions of Pei & Fall (1995) from models of cosmic chemical evolution. The circles at $z = 0, 0.2$, and 0.875 are from the H α surveys by Gallego et al. (1995), Tresse & Maddox (1998), and Glazebrook et al. (1999), respectively. The squares are from the ISO 15 μm survey by Flores et al. (1999). The circle with an arrow at $z \approx 3$ is from the SCUBA submillimeter observations by Hughes et al. (1998).

global rate of star formation are robust at $z \lesssim 2$, but still uncertain by a factor of three at $z \gtrsim 3$. The robustness at $z \lesssim 2$ is due to the tight constraint imposed by the cosmic infrared background on how much radiation is emitted and absorbed at shorter wavelengths. At $z \gtrsim 3$, there is little time to accumulate much radiation in the background. Consequently, the observed background provides only a weak constraint on the star formation rates at high redshifts. Our models indicate that the rest-frame emissivity of galaxies evolves strongly not only in the near-ultraviolet (e.g., 2800 \AA) but also in the far-infrared (e.g., 100 μm). Either one of these emissivities, if studied in isolation, would provide only a partial tracer of star formation. The most promising way to determine the global rates of star formation at $z \gtrsim 3$ will be to combine future near-infrared and submillimeter surveys; the former traces the direct radiation from stars at rest-frame near-ultraviolet wavelengths, while the latter traces the reradiation by dust at rest-frame far-infrared wavelengths. For $z \gtrsim 4$, stellar emission at $\lambda = 2800 \text{ \AA}$ is redshifted to $\lambda \gtrsim 1.4 \mu\text{m}$, and falls within the window of the Next Generation Space Telescope (NGST), whereas dust emission at $\lambda = 100 \mu\text{m}$ is redshifted to $\lambda \gtrsim 500 \mu\text{m}$, and falls within the window of the Millimeter Array (MMA). Thus, a combination of these two instruments should eventually enable us to trace the global history of star formation to high redshifts.

4.4. Evolution of Galaxies

Our models of cosmic chemical evolution provide a global description of the major constituents of galaxies. Figure 14 shows the inferred evolution of the stars, interstellar gas, baryons in galaxies, and baryon flow between the interstellar and intergalactic media. The data point $\Omega_s = (4.9^{+3.1}_{-2.2}) \times 10^{-3}$ at $z = 0$ is an estimate from the observed mean B -band emissivity of nearby galaxies and the mean mass-to-light ratios in spheroids, disks, and irregular galaxies (Fukugita, Hogan, & Peebles 1998), while the data point $\Omega_g = (5.0 \pm 1.2) \times 10^{-4}$ at $z = 0$ comes from observations of the 21 cm emission of nearby galaxies (§ 2.2.6). The results from our models are plotted as the curves in each panel of Figure 14. The agreement with $\Omega_g(0)$ is by design, while the agreement with $\Omega_s(0)$ is an indication that our adopted lower mass cutoff in the IMF is reasonable. Evidently, galaxies contain mostly stars at $z \lesssim 1$ and mostly gas at $z \gtrsim 2$. The bulk of the stars seen today formed at relatively low redshifts: 34 – 48% since $z = 1$, 72 – 91% since $z = 2$, 91 – 98% since $z = 3$, and 97 – 99% since $z = 4$.

Although there are still significant uncertainties in

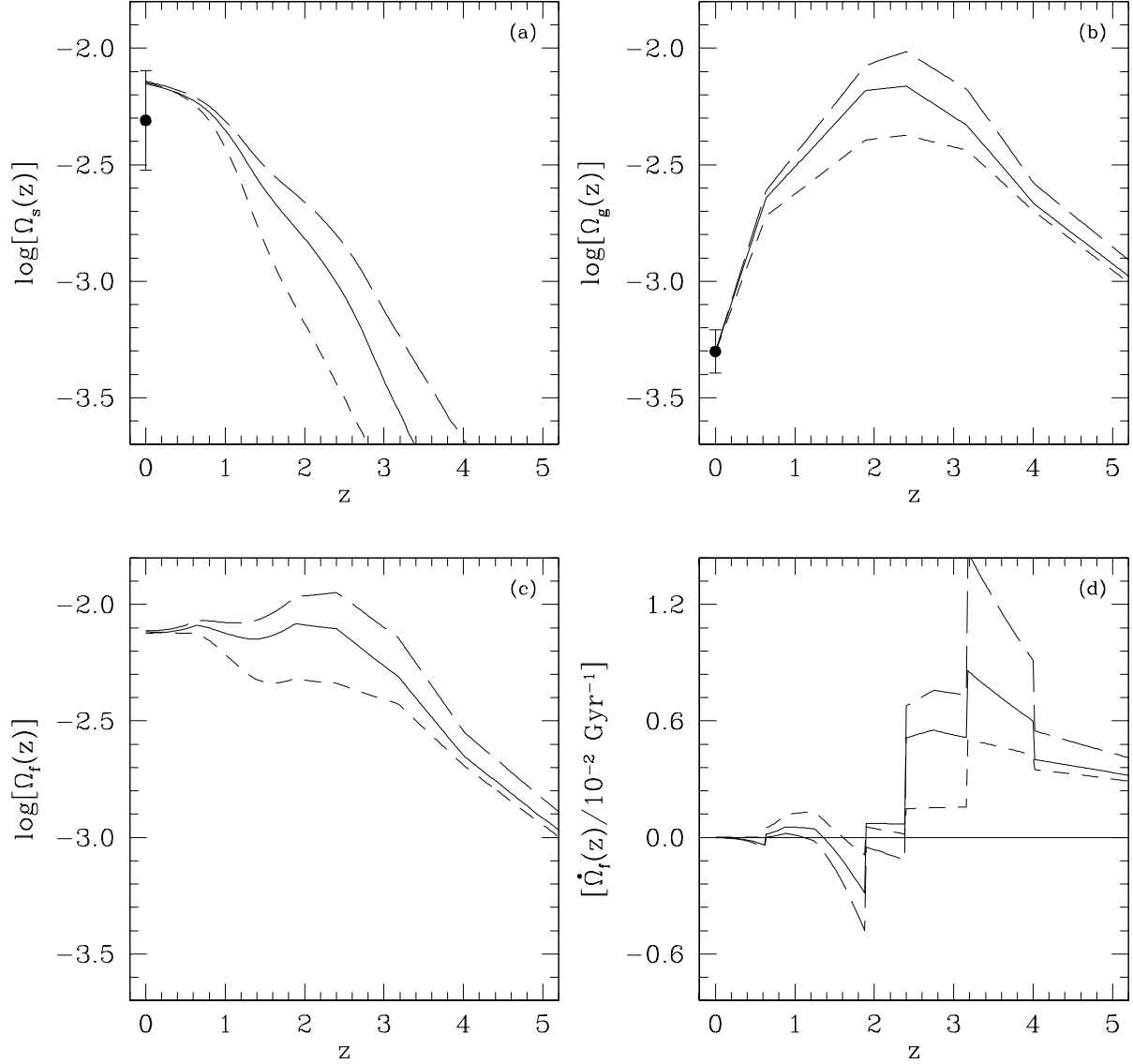


FIG. 14.—Evolution of (a) the comoving density of stars, (b) the comoving density of interstellar gas, (c) the comoving density of baryons in galaxies, and (d) the comoving rate of baryon flow between the interstellar and intergalactic media. The solid, short-dash, and long-dash curves are the best, minimum, and maximum solutions in our models. The data point for $\Omega_s(0)$ is an estimate from the mean blue luminosity density and mass-to-light ratio of nearby galaxies (Fukugita et al. 1998), while the data point for $\Omega_g(0)$ is inferred from 21 cm emission observations of nearby galaxies (§ 2.2.6).

these solutions, they can be divided roughly into three periods: (1) At $z \gtrsim 3$, there is a rapid inflow from the intergalactic medium and hence a build up of the interstellar gas within galaxies (Figs. 14b and 14c). (2) At $1 \lesssim z \lesssim 3$, the interstellar gas content is high (Fig. 14b), presumably triggering high rates of star formation (Fig. 13). This in turn causes the rapid accumu-

lation of stars (Fig. 14a) and heavy elements (Fig. 8), and strong emission from stars and dust (Fig. 9). (3) At $z \lesssim 1$, the stellar content continues to increase but at a slower rate, while the gas content (Fig. 14b), star formation rate (Fig. 13), ultraviolet and optical stellar emission (Fig. 9), and far-infrared dust emission (Fig. 9) all decrease. During this period, the interstellar gas is

consumed by star formation without much replenishment by inflow. Our results therefore suggest that, on average, galaxies spend 13 – 18% of their lives (defined by the present age of the universe) in a “growth” period, 23 – 25% of their lives in a “working” period, and 64 – 57% of their lives in a “retirement” period (for $\Lambda = 0$ and $0.1 \leq q_0 \leq 0.5$).

It appears from our models that the most significant inflow occurred at $z \approx 3 - 4$ (Fig. 14d). This inference, however, depends crucially on the estimates of $\Omega_{\text{HI}o}$ from damped Ly α surveys at the highest redshifts (Fig. 7a). If the observed HI content were underestimated at $z \gtrsim 3$, the peak in the inflow could be pushed to an earlier epoch. Since the interstellar metallicity is inversely proportional to the comoving density of gas, the observed metallicity at $z \approx 3 - 4$ also provide a constraint on the peak in the inflow. Therefore, better determinations of the comoving density of HI and mean metallicity in the damped Ly α systems at $z \gtrsim 3$ would help reduce the uncertainties in the epoch when the bulk of the interstellar gas was assembled in galaxies.

In most models based on hierarchical clustering, including the cold dark matter model, galaxies form relatively late. The exact evolution depends on a large number of processes, including the merging of dark matter halos, the gravitational heating and radiative cooling of gas within them, the formation of stars, the feedback of stellar mass, energy, and metals to the interstellar medium, and so forth. Semianalytical models treat these processes by simple, physically-motivated recipes; and with suitable choices of parameters, they are found to be consistent with many of the observed properties of galaxies (White & Frenk 1991; Kauffmann, White, Guiderdoni 1993; Cole et al. 1994; Somerville & Primack 1998). In some semianalytical models, the comoving rate of star formation and the comoving density of cold gas rise to peak values at $z \approx 1 - 2$ and then decline at lower redshifts (Kauffmann 1996; Baugh et al. 1998). These models are therefore qualitatively consistent with our models of cosmic chemical evolution and the observations on which they are based. The evolution of $\dot{\Omega}_s$ and Ω_g in the semianalytical models is, however, milder than the observed evolution. It is not yet clear whether or not this represents a significant discrepancy.

4.5. Chemical Enrichment of the Intergalactic Medium

The chemical enrichment of the intergalactic medium could be the result of an outflow of metal-enriched gas from galaxies or nucleosynthesis in objects much smaller and more uniformly distributed than galaxies (e.g., pregalactic stars or star clusters). We explore in this section the possibility of outflows from galaxies. To do so, we

write the comoving density of metals in the intergalactic medium as

$$\Omega_{\text{mIGM}}(z) = \int_z^\infty dz' \left| \frac{dt}{dz'} \right| \dot{\Omega}_O(z') Z(z'), \quad (45)$$

where $\dot{\Omega}_O$ is the comoving rate of outflow from galaxies and Z is the mean metallicity of the outflowing gas. The net flow rate discussed in § 2.1 is simply $\dot{\Omega}_f = \dot{\Omega}_I - \dot{\Omega}_O$, where $\dot{\Omega}_I$ is the comoving rate of inflow. Both $\dot{\Omega}_O$ and $\dot{\Omega}_I$ must be positive, whereas $\dot{\Omega}_f$ can be positive or negative. We assume, as a good approximation, that $\dot{\Omega}_O = -\dot{\Omega}_f$ for $\dot{\Omega}_f < 0$ (by ignoring any inflow if the net flow is dominated by outflow) and $\dot{\Omega}_O = \eta \dot{\Omega}_f$ for $\dot{\Omega}_f > 0$ with $\eta \ll 1$ (to allow for some outflow if the net flow is dominated by inflow). A small but non-zero value of η only affects equation (3) in § 2.1. We have checked that all of the results presented in § 3 are nearly the same for $\eta \lesssim 0.3$, with a maximum difference of less than 20% in Z . In this case, we can make rough estimates of the chemical enrichment of the intergalactic medium from our solutions for the net rate of baryon flow.

Figure 15 shows the mean comoving density of metals in the intergalactic medium, resulting from the outflow of metal-enriched gas from galaxies in our models. The three curves represent our three solutions with $\eta = 0.2$.

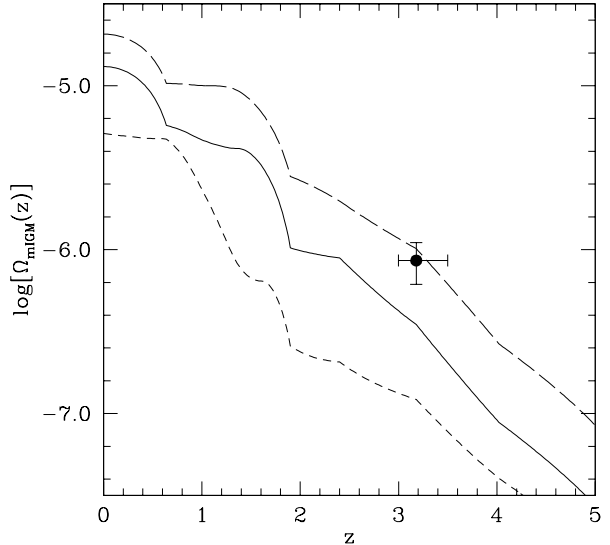


FIG. 15.—Mean comoving density of metals expelled from galaxies into the intergalactic medium as a function of redshift. The solid, short-dash, and long-dash curves are the best, minimum, and maximum solutions in our models. The data point at $z = 3.2$ was derived by Songaila (1997) from observations of C IV and Si IC absorption lines in the Ly α forest with some ionization corrections and assumptions about relative abundances.

The data point at $z = 3.2$ was derived by Songaila (1997) from observations of C IV and Si IV absorption lines in the Ly α forest (corresponding roughly to $N_{\text{HI}} \lesssim 10^{17} \text{ cm}^{-2}$) with some modest ionization corrections and assumptions about the relative abundances of different elements. Although the data and models are both uncertain, the rough agreement indicates that even a small outflow of metal-enriched gas from galaxies could account for the observed metal content of the Ly α forest. A comparison of Figure 15 with Figure 8 suggests that the comoving density of intergalactic metals is typically an order of magnitude smaller than that of interstellar metals and that the two are comparable only at $z \lesssim 0.4$. This is nearly independent of the relative outflow rate for $\eta \lesssim 0.3$. Galaxies probably retained most of their metals up until now, but there could be almost as many metals in the intergalactic medium as in the interstellar media of galaxies at $z = 0$.

The global mean metallicity of the intergalactic medium is $\langle Z_{\text{IGM}} \rangle = \Omega_{\text{mIGM}}/\Omega_{\text{gIGM}}$, where Ω_{gIGM} is the total gas content in the intergalactic medium. Adopting $\Omega_{\text{gIGM}} \approx 0.02$ from Big Bang nucleosynthesis (Fukugita et al. 1998), we estimate $\log \langle Z_{\text{IGM}}/Z_{\odot} \rangle \approx -1.5, -2.6$, and -3.6 at $z = 0, 2$, and 4 , respectively. We emphasize, however, that there could be a large dispersion around the mean, depending on whether and how much the metals expelled from galaxies are mixed with the intergalactic medium. If the metals were mixed completely with all of the intergalactic gas, the metallicity would be the same everywhere, i.e., $Z_{\text{IGM}} = \langle Z_{\text{IGM}} \rangle$. If the metals (and gas) were not mixed at all in the intergalactic medium, the metallicity would fluctuate between $Z_{\text{IGM}} = Z$ in regions where the ejected gas is present and $Z_{\text{IGM}} = 0$ in regions where it is not present. Some degree of inhomogeneity would seem to be the most likely situation.

5. CONCLUSIONS

We have studied the global evolution of the stellar, gaseous, and metal contents of galaxies, as well as the radiation they emit and the baryon flow between the interstellar and intergalactic media. Our results are based on models of cosmic chemical evolution, with observational inputs from damped Ly α absorption-line surveys and optical imaging and redshift surveys, and measurements of the cosmic infrared background. The novel feature of our approach is a self-consistent treatment of the obscuration, absorption, and emission by dust. We emphasize that all of our results pertain to the mean properties of galaxies, averaged over comoving volumes large enough to be fair samples of galaxies of all masses, sizes, and morphological types. Such a global approach

has the advantage of simplicity, but the disadvantage that many interesting questions concerning the diversity of galaxies cannot be addressed. In particular, our results are completely independent of the unknown morphologies, sizes, and space densities of the damped Ly α systems.

We find that the extragalactic far-infrared background detected by the *COBE* DIRBE and FIRAS can be accounted for if much of the radiation emitted by stars is absorbed and reemitted by small-scale clumps of dust, possibly associated with individual stars. The ratio of the bolometric dust emission to the bolometric stellar emission in our models increases from 36% at $z = 0$ to about 60% at $z \approx 1$ and becomes uncertain at higher redshifts (10–70% at $z \gtrsim 3$). Of the total energy radiated by stars (integrated over all redshifts), 41–46% is in the ultraviolet/optical/near-infrared part of extragalactic background, while the remaining 59–54% is in the mid-infrared/far-infrared/submillimeter part. The absorption by dust corrects the global rates of star formation inferred from optical surveys upward by factors of 2.5, 3–4, and 2–8 at $z = 0, 1$, and 3 , respectively. From our models, it appears that galaxies may have experienced a sustained period of intense star formation at $1 \lesssim z \lesssim 3$ and somewhat less rapid star formation at $z \lesssim 1$ and $z \gtrsim 3$, roughly correlated with the evolution of their neutral gas content, although the evolution at $z \gtrsim 3$ is quite uncertain. We note, however, that if the global rate of star formation were to remain high beyond $z \approx 3$, it would produce more metals in the interstellar medium than are observed in the damped Ly α systems, unless a significant outflow had occurred before $z \approx 3$.

The solutions presented here for the mean properties of galaxies are based on relatively few input observations, but they match remarkably well a wide variety of other observations, mostly within the quoted 1σ errors of the data. In particular, our models reproduce: (1) the extragalactic background derived from galaxy counts at $\lambda = 0.2\text{--}2.2 \mu\text{m}$; (2) the rest-frame 0.44, 1.0, and $2.2 \mu\text{m}$ emissivities from the available surveys of galaxies up to $z \approx 2$; (3) the infrared dust emissivities from nearby galaxies at $\lambda = 12, 25, 60$, and $100 \mu\text{m}$; (4) the observed mean abundance of heavy elements in the damped Ly α systems at $0.4 \lesssim z \lesssim 3.5$; and (5) the global rates of star formation inferred from H α and ISO mid-infrared surveys at $z \lesssim 1$ and recent SCUBA submillimeter observations. The metal enrichment history of the intergalactic medium implied by our models is also consistent with the observed mean comoving density of metals in the Lyman-alpha forest at high redshifts. Our solutions are robust at $z \lesssim 2$ but uncertain at $z \gtrsim 3$. Major sources of uncertainties are the optical opacity of grains and the small-scale clumpiness of dust in the interstellar

medium. Both of these are likely to remain uncertain for some time and hence will affect the interpretations of future optical and infrared observations as well.

Our results indicate that many different observations of galaxies, by means of quasar absorption lines, optical imaging and redshift surveys, and extragalactic background measurements, can be brought together to provide a coherent picture of the global evolution of galaxies over much of the Hubble time. The models presented here suggest that the process of galaxy formation may have undergone different evolutionary phases: (1) an early period of significant inflow to assemble interstellar gas at $z \gtrsim 3$; (2) a subsequent period of intense star formation and chemical enrichment at $1 \lesssim z \lesssim 3$; and (3) a recent period of decline in the gas content, star formation rate, and the ultraviolet and optical stellar emissivity, and far-infrared dust emissivity at $z \lesssim 1$. Currently, there are still large uncertainties in this picture, especially at $z \gtrsim 3$. Future surveys that aim to trace the rest-frame near-ultraviolet emissivity of stars, the rest-frame far-infrared emissivity of dust, and the global properties of interstellar gas, heavy elements, and dust beyond $z \approx 3$ could reduce these uncertainties and thus advance our knowledge of the global evolution of galaxies.

We thank Rick Arendt, Stéphane Charlot, Mark Dickinson, Eli Dwek, Piero Madau, and Nino Panagia for helpful discussions. We are grateful to Stéphane Charlot for providing his latest stellar population synthesis models, to Lisa Storrie-Lombardi for communicating the redshift path information of the damped Ly α sample, and to Dale Fixsen for making the unpublished errors in the FIRAS data available to us. M.G.H and Y.C.P acknowledge *COBE* project support from NASA grant NAG 5-3899.

REFERENCES

- Armand, C., Milliard, B., & Deharveng, J.M. 1994, *A&A*, 284, 12
- Barger, A.J., Cowie, L.L., Sanders, D.B., Fulton, E., Taniguchi, Y., Sato, Y., Kawara, K., & Okuda, H. 1998, *Nature*, 394, 248
- Baugh, C.M., Cole, S., Frenk, C.S., & Lacey, C.G. 1998, *ApJ*, 498, 504
- Biller, S.D., Buckley, J., Burdett, A., Gordo, J.B., Carter-Lewis, D.A., Fegan, D.J., Findley, J., Gaidos, J.A., Hillas, A.M., Krennrich, F., Lamb, R.C., Lessard, R., McEnery, J.E., Mohanty, G., Quinn, J., Rodgers, A.J., Rose, H.J., Samuelson, F., Sembroski, G., Skelton, P., Weekes, T.C., & Zweerink, J. 1998, *Phys. Rev. Lett.*, 80, 2992
- Blain, A.W., Smail, I., Ivison, R.J., & Kneib, J.-P. 1999, *MNRAS*, 302, 632
- Boissé, P., Le Brun, V., Bergeron, J., & Deharveng, J.-M. 1998, *A&A*, 333, 841
- Bowyer, S. 1991, *ARA&A*, 29, 59
- Bruzual, A., & Charlot, S. 1998, in preparation
- Calzetti, D., & Heckman, T.M. 1999, *ApJ*, in press, astro-ph/9811099
- Cole, S., Aragon-Salamanca, A., Frenk, C.S., Navarro, J.F., & Zepf, S.A. 1994, *MNRAS*, 271, 781
- Connolly, A.J., Szalay, A.S., Dickinson, M., Subbarao, M.U., & Brunner, R.J. 1997, *ApJ*, 486, L11
- Cowie, L.L., Songaila, A., Hu, E.M., & Cohen, J.G. 1996, *ApJ*, 112, 839
- Désert, F.X., Boulanger, F., Puget, J.L. 1990, *A&A*, 237, 215
- Draine, B.T., & Lee, H.M. 1984, *ApJ*, 285, 89
- Dube, R.R., Wickes, W.W., & Wilkinson, D.T. 1979, *ApJ*, 232, 333
- Dwek, E. 1998, *ApJ*, 501, 643
- Dwek, E., & Arendt, R.G. 1998, *ApJ*, 508, L9
- Dwek, E., Arendt, R.G., Hauser, M.G., Fixsen, D., Kelsall, T., Leisawitz, D., Pei, Y.C., Wright, E.L., Mather, J.C., Moseley, S.H., Odegard, N., Shafer, R., Silverberg, R.F., & Weiland, J.L. 1998, *ApJ*, 508, 106
- Ellis, R.S., Colless, M., Broadhurst, T., Heyl, J., & Glazebrook, K. 1996, *MNRAS*, 280, 235
- Fall, S.M. 1998, in *Hubble Deep Field*, ed. M. Livio, S.M. Fall, & P. Madau (Cambridge: Cambridge University Press), 163
- Fall, S.M., Charlot, S., & Pei, Y.C. 1996, *ApJ*, 464, L43
- Fall, S.M., & Pei, Y.C. 1993, *ApJ*, 402, 479
- Fixsen, D.J., Cheng, E.S., Gales, J.M., Mather, J.C., Shafer, R.A., & Wright, E.L. 1996, *ApJ*, 473, 576
- Fixsen, D.J., Dwek, E., Mather, J.C., Bennett, C.L., & Shafer, R. 1998, *ApJ*, 508, 123
- Flores, H., F. Hammer, F., Thuan, T., Césarsky, C., Désert, F.X., Omont, A., Lilly, S.J., Eales, S., Cramp-ton, D., & Le Fèvre, O. 1999, *ApJ*, in press, astro-ph/9811202
- Fukugita, M., Hogan, C.J., & Peebles, P.J.E. 1998, *ApJ*, 503, 518
- Gallego, J., Zamorano, J., Aragón-Salamanca, A., & Regg, M. 1995, *ApJ*, 455, L1
- Gardner, J.P., Sharples, R.M., Frenk, C.S., & Carrasco, B.E. 1997, *ApJ*, 480, 99
- Ge, J., & Bechtold, J. 1997, *ApJ*, 477, L73
- Glazebrook, K., Blake, C., Economou, F., Lilly, S., & Colless, M. 1999, *MNRAS*, in press, astro-ph/9808276
- Hacking, P.B., & Soifer, B.T. 1991, *ApJ*, 367, L49
- Hartwick, F.D.A., & Schade, D. 1990, *ARA&A*, 28, 437

- Hauser, M.G., Arendt, R.G., Kelsall, T., Dwek, E., Odegard, N., Weiland, J.L., Freudenreich, H.T., Reach, W.T., Silverberg, R.F., Moseley, S.H., Pei, Y.C., Lubin, P., Mather, J.C., Shafer, R.A., Smoot, G.F., Weiss, R., Wilkinson, D.T., & Wright, E.L. 1998, *ApJ*, 508, 25
- Hogan, C.J., Oliver, K.A., & Scully, S.T. 1997, *ApJ*, 489, L119
- Holberg, J. 1986, *ApJ*, 311, 969
- Hughes, D., Serjeant, H., Dunlop, J., Rowan-Robinson, M., Blair, A., Mann, R.G., Ivison, R., Peacock, J., Efsthathiou, A., Gear, W., Oliver, S., Lawrence, A., Longair, M., Goldschmidt, P., Jenness, T. 1998, *Nature*, 394, 241
- Kashlinsky, A., Mather, J.C., Odenwald, S. 1996, *ApJ*, 473, L9
- Kauffmann, G. 1996, *MNRAS*, 281, 475
- Kauffmann, G., White, S.D.M., & Guiderdoni, B. *MNRAS*, 264, 201
- Kulkarni, V.P., S.M., Fall, & Truran, J.W. 1997, *ApJ*, 484, L7
- Lanzetta, K.M., Wolfe, A.M., & Turnshek, D.A. 1995, *ApJ*, 440, 435
- Lanzetta, K.M., Wolfe, A.M., Turnshek, D.A., Lu, L., McMahon, R.G., & Hazard, C. 1991, *ApJS*, 77, 1
- Le Brun, V., Bergeron, J., Boissé, P., & Deharveng, J.M. 1997, *A&A*, 321, 733
- Leitherer, C., Ferguson, H.C., Heckman, T.M., & Lowenthal, J.D. 1995, *ApJ*, 454, L19
- Levshakov, S.A., Chaffee, F.H., Foltz, C.B., & Black, J.H. 1992, *A&A*, 262, 385
- Lilly, S.J., Eales, S.A., Gear, W.K.P., Hammer, F., Le Fevre, O., Crampton, D., Bond, J.R., & Dunne, L. 1999, *ApJ*, in press, astro-ph/9901047
- Lilly, S.J., Le Fèvre, O., Hammer, F., & Crampton, D. 1996, *ApJ*, 460, L1
- Lilly, S.J., Tresse, L., Hammer, F., Crampton, D., & Le Fèvre, O. 1995, *ApJ*, 455, 108
- Luck, R.E., & Lambert, D.L. 1992, *ApJS*, 79, 303
- Madau, P., Ferguson, H.C., Dickinson, M.E., Giavalisco, M., Steidel, C.C., & Fruchter, A. 1996, *MNRAS*, 283, 1388
- Madau, P., Pozzetti, L., & Dickinson, M. 1998, *ApJ*, 498, 106
- Natta, A., & Panagia, N. 1984, *ApJ*, 287, 228
- Ostriker, J.P., & Heisler, J. 1984 *ApJ*, 278, 1
- Pei, Y.C. 1992, *ApJ*, 395, 130
- Pei, Y.C. 1995, *ApJ*, 438, 623
- Pei, Y.C., & Fall, S.M. 1995, *ApJ*, 454, 69
- Pei, Y.C., Fall, S.M., & Bechtold, J. 1991, *ApJ*, 378, 6
- Perna, R., Loeb, A., & Bartelmann, M. 1997, *ApJ*, 488, 550
- Pettini, M., King, D.L., Smith, L.J., & Hunstead, R.W. 1997a, *ApJ*, 478, 536
- Pettini, M., Smith, L.J., Hunstead, R.W., & King, D.L. 1994, *ApJ*, 426, 79
- Pettini, M., Smith, L.J., King, D.L., & Hunstead, R.W. 1997b, *ApJ*, 486, 665
- Pozzetti, L., Madau, P., Ferguson, H.C., Zamorani, G., & Bruzual, G.A. 1998, *MNRAS*, 298, 1133
- Puget, J.-L., Abergel, A., Bernard, J.-P., Boulanger, F., Burton, W.B., Désert, F.-X., & Hartmann, D. 1996, *A&A*, 308, L5
- Rao, S., & Briggs, F. 1993, *ApJ*, 419, 515
- Reiss, A.G., et al. 1998, *AJ*, 116, 1009
- Schegel, D.J., Finkbeiner, D.P., & Davis, M. 1998, *ApJ*, 500, 525
- Shaver, P.A., Wall, J.V., Kellermann, K.I., Jackson, C.A., & Hawkins, M.R.S. 1996, *Nature*, 384, 439
- Smette, A., Claeskens, J.-F., & Surdej, J. 1997, *New Astronomy*, 2, 53
- Soifer, B.T., & Neugebauer, G. 1991, *AJ*, 101, 354
- Somerville, R.S., & Primack, J.R. 1998, *MNRAS*, submitted, astro-ph/9802268
- Songaila, A. 1997, *ApJ*, 490, L1
- Stanev, T., & Franceschini, A. 1998, *ApJ*, 494, 159
- Steidel, C.C., Adelberger, K.L., Giavalisco, M., Dickinson, M., & Pettini, M. 1999, *ApJ*, in press, astro-ph/9811399
- Steidel, C.C., Giavalisco, M., Pettini, M., Dickinson, M., & Adelberger, K.L. 1996, *ApJ*, 462, L17
- Storrie-Lombardi, L.J., Irwin, M.J., & McMahon, R.G. 1996a, *MNRAS*, 282, 1330
- Storrie-Lombardi, L.J., McMahon, R.G., & Irwin, M.J. 1996b, *MNRAS*, 283, L79
- Tinsley, B.M. 1980, *Fund. Cosmic Phys.*, 5, 287
- Toller, G.N. 1983, *ApJ*, 266, L79
- Tresse, L., & Maddox, S.J. 1998, *ApJ*, 495, 691
- Vladilo, G. 1998, *ApJ*, 493, 583
- White, S.D.M., & Frenk, C.S. 1991, *ApJ*, 379, 52
- Williams, R.E., Blacker, B., Dickinson, M., van Dyke, W., Ferguson, H.C., Fruchter, A.S., Giavalisco, M., Gilliland, R.L., Heyer, I., Katsanis, R., Levey, Z., Lucas, R.A., McElroy, D.B., Petro, L., & Postman, M. 1996, *AJ*, 112, 1335
- Wolfe, A.M., Turnshek, D.A., Smith, H.E., & Cohen, R.D. 1986, *ApJS*, 61, 249
- Wolfe, A.M., Lanzetta, K.M., Foltz, C.B., & Chaffee, F.H. 1995, *ApJ*, 454, 698
- Young, J.S., & Scoville, N.Z. 1991, *ARA&A*, 29, 581
- Zwaan, M.A., Briggs, F.H., Sprayberry, D., & Sorar, E. 1997, *ApJ*, 490, 173